공학박사 학위논문

Risk Management of Chemical Processes Using Dynamic Simulation and CFD-based Surrogate Model Approach

동적 시뮬레이션과 전산유체역학 기반의 대리 모델 접근법을 통한 화학공정의 위험도 관리

2020년 2월

서울대학교 대학원

화학생물공학부

고 창 준

Abstract

Risk Management of Chemical Processes Using Dynamic Simulation and CFD-based Surrogate Model Approach

Changjun Ko
School of Chemical & Biological Engineering
The Graduate School of Seoul National University

Process safety has been considered as one of the most important factors to manage a chemical plant due to a vast amount of damage in case of accidents. To achieve this goal, several methodologies have been introduced by various studies, e.g., hazard and operability (HAZOP) study, layer of protection analysis (LOPA), event tree analysis (ETA), bow-tie analysis, quantitative risk assessment (QRA), etc. The methodologies mentioned above are usually performed by commercial software which can provide each of accident or process information. However, since process

and accident are closed related to each other, these two modules should be integrated to produce a quantitative and accurate risk outcome can result in the reliable process management. Thus, new methodologies to manage a heavy oil desulfurization (HOD) process by integrating process and accident simulations are proposed in this paper.

First, a methodology for quantitative risk assessment (QRA) integrated with dynamic simulation and accident simulation is proposed for the purpose of discovering inherent risks which are undetectable by the conventional method. For this, a dynamic simulation of shut-down procedure in the HOD process is performed to observe the behavior of process variables with the commercial software of Aspen HYSYS and from the dynamic simulation results, several blind spots that shows higher operating pressure than the steady-state simulation are identified. To assess the risks of the detected blind spots, QRA are performed using SAFETI. As a result of applying the proposed method to HOD process, several spots, which was identified as having low risks, turned out to be intolerably risky. In addition, mitigation procedures are carried out which reduces the risk of the process to the tolerable level, resulting in a safer and more reliable process.

Secondly, to safely operate the HOD process, a new operator training system (OTS) which targets the interactive cooperation of control room operators (CROPs) and field operators (FOPs) was introduced with the aid of data transfer between process and accident simulation results. This interactive simulation module induces the CROPs and FOPs to take proper actions in case of accident situation among pre-identified scenarios in a chemical plant. Developed model integrates the real-time

process dynamic simulation by Aspen HYSYS with the off-line database of 3D-computational fluid dynamics (CFD) accident simulation results by FLACS in a designed interface using object linking and embedding (OLE) technology. As a result, an improved training effect is expected by providing accurate process and accident information to both CROPs and FOPs in real-time.

Lastly, a surrogate model which consists of dimensionality reduction and generating a regression model is introduced to replace the high-cost CFD-based FLACS model. The dimensionality reduction is performed by a variational autoencoder (VAE) combined with deep convolutional layers (DN). Through this method, the CFD results are compressed in the latent space by a probabilistic encoder. In sequence, input variables are mapped to the latent space with the aid of a deep neural network (DNN), resulting in an efficient regression model. Then this regression model is reconstructed by a probabilistic decoder, to successfully substitute the original CFD image.

Keywords: Heavy oil desulfurization; Dynamic simulation; Quantitative risk assessment; Operator training system; Computational fluid dynamics; Surrogate model; Variational autoencoder

Student ID: 2015-21036

Contents

List of figures

List of tables

Chapter 1. Introduction

1.1. Research motivation

The scale of chemical industries have been expanded in last few decades at an alarming due to the increased demand on various derivative products. Thus, the concern that manage chemical processes safely also became a big issue to prevent the vast damage in case of accidents. However, owing to the complexity of various factors such as chemical components, layout of plants, etc., it is highly tough to operate chemical processes on the basis of quantitative risk calculations.

Recently, several studies have been introduced to resolve these bottlenecks. The representative methodologies, for example, are hazard and operability (HAZOP) study, layer of protection analysis (LOPA), event tree analysis (ETA), bow-tie analysis, and quantitative risk assessment (QRA). In most cases, simulations with commercial software are accompanied to quantitatively assess the risk outcomes. One of the widely used tools is Aspen HYSYS which provide process information and other tools also exist such PHAST and FLACS which provide 2D and 3D accident information respectively.

Usually, these tools are used individually, to be disadvantages in that only one of the process and accident information is provided. However, process and accident are closely related to each other in real situations, therefore, these two modules should be integrated to serve comprehensive knowledge of the entire process form process anomalies to catastrophic accidents. In this point of view, several methodologies are proposed in this paper to accomplish linkage of process and accident.

1.2. Target process description

The heavy oil desulfurization (HOD) process is designed to remove impurities such as sulfur, nitrogen and other metal contained in heavy oil. It had been constructed and currently being operated in Seosan city, South Korea with a capacity of 66,000 barrel/Day feed rate. The HOD process consists of several subsections, which are showed in Figure 1-1. In the reactor section, the reactant compounds including sulfur and other impurities are hydrogenated with the aid of nickel, cobalt and other metal catalysts to be hydrogen sulfide and hydrocarbons. The representative reactions are expressed as below:

$$R_2CHSH + H_2 \xrightarrow[Catalyst]{} R_2CH_2 + H_2S \quad (1\text{-}1)$$

$$Thiophene + 4H_2 \xrightarrow[Catalyst]{} Paraffin + H_2S \quad (1\text{-}2)$$

The latter part consists of several sections for recycling the unreacted hydrogen and separating the product. As can be seen in Figure 1-1, since the operating conditions of the HOD process is quite harsh, when accidents happens, a great amount of damage can be caused which severely affect not only the process itself but also the surrounding processes. Therefore, is was reasonably chosen as the target process of analysis.

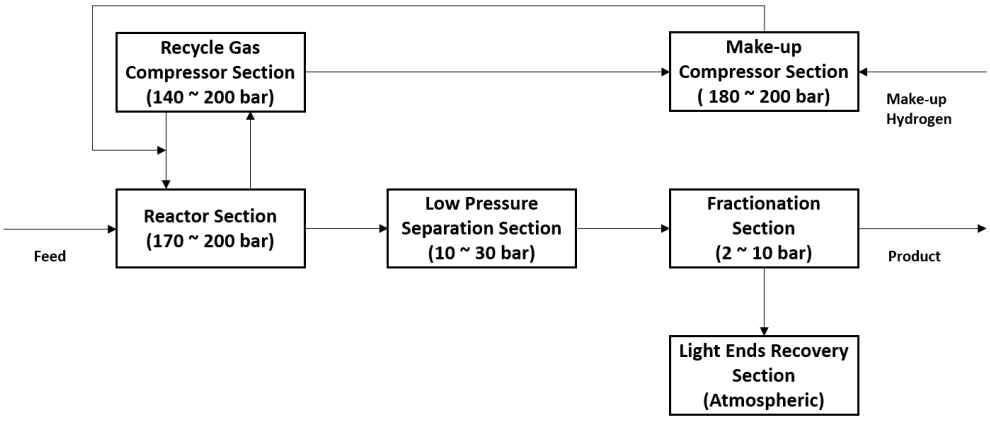

Figure 1-1. Block flow diagram of HOD process

1.3. Outline of the thesis

Chapter 1 introduces the research motivation of short description about the targeted HOD process. In Chapter 2, a QRA is performed on the basis of multi-unit dynamic simulation with 2D accident simulation to detect potential blind spots which would be undetectable in steady-state conditions. In Chapter 3, an operator training system (OTS) is developed with a combination of plant-wide dynamic simulation, 3D accident simulation, and a platform through which process/accident data are transferred. In Chapter 4, a surrogate model based on a variational autoencoder with deep convolutional layers is constructed for the application of the results of Chapter 3 in real-time. In Chapter 5, the contribution of the studies in this paper is arranged sequentially, and conclusion is presented.

Chapter 2. Multi-unit dynamic simulation with 2D accident simulation: Implementation of quantitative risk assessment

2.1. Introduction

The primary goal of quantitative risk assessment (QRA) is to provide tools for reducing acute risks in a plant handling hazardous materials. The quantitative estimation of risk enables management to identify major risk contributors and the outcome of various risk reduction options. [1] QRA was firstly proposed in the field of nuclear industry in the 1970's due to their vast damage in case of accidents. However, it is now widely used in various fields such as natural science, engineering, medicine, etc. Furthermore, many new methodologies are still being developed regarding QRA. [2] Most studies mainly focus on consequence-based probabilistic methodologies which are considered general in QRA. [3] [4] [5] In recent years, a variety of approaches have emerged that go beyond traditional methodologies, which focus more on the feasibility, reliability and accuracy of risk assessment methods. Khakzad et al. [6] illustrated the use of Bayesian networks in both accident occurrence probability estimation and updating in the light of new information. There are also many attempts to use computational fluid dynamics (CFD) calculations to accurately model three-dimensional toxic gas diffusion and flammable gas explosion results. Middha et al. [7] performed a number of CFD simulations of selected scenarios of impinging jet gas dispersion and subsequent gas

explosion with commercial software and carried out validation on those models. Jung et al. [8] demonstrated a systematic technique to integrate QRA in the optimization of plant layout by three methodologies: a fixed distance approach, an overpressure-based approach, and integration of two approaches. Yet-pole et al. [9] employed a CFD model to simulate the fire and explosion consequences of three worst-case scenarios within a complex naphtha-cracking process area.

2.2 Background

Since accident results are closely related to process variables, there have been other attempts of QRA studies which linked process simulations with accident simulations. Domenico et al. [10] illustrated the advantages of integrating process simulation and QRA to investigate the acceptability of a new technology for a methanol production plant. Lee et al. [11] deduced the concept of static inventory to apply the behavior of the process fluid in normal process simulation to accident simulation for a gas treatment unit, and calculated the new operating conditions using the process simulation. All the aforementioned studies used steady-state models for process simulation as tools for calculating quantitative risks by simulating accidental situations: Domenico et al. [10] considered the simulation study of normal and worst-case operations, and Lee et al. [11] took into account steady-state process simulation to assess the potential risk at the preliminary design stage. Since they analyzed risks based on steady-state simulation, potential risks caused by momentarily increased pressure or temperature of process units during certain operations cannot be captured.

As dynamic simulation can quantitatively monitor the varying conditions of various process units depending on time, the results can be used to analyze and apprehend the inherent process behavior for applying them to the

process and equipment design or real-time optimization of the process. Also, dynamic simulation can be utilized for designing safety systems such as alarms, overrides, interlocks and relief valves as it can offer dynamic responses of the process under various failure scenarios. [12] In this point of view, researchers have recently developed methods to perform safety analysis with dynamic simulations. [13] [14] Lou et al. [15] simulated a large-scale ethylene oxide manufacturing process to discover safety zone boundaries. Eizenberg et al. [16] conducted a hazard and operability (HAZOP) [17] [18] study to find the magnitude of the deviations from normal operating conditions and tested design alternatives to improve the safety characteristic of an exothermic reaction process. Furthermore, Berdouzi et al. [19] suggested a methodology which combines HAZOP-based dynamic simulations with risk matrices to perform the semi-quantitative risk analysis for an exothermic reaction.

The studies reviewed above have focused on the deviations of operating conditions when process malfunctions happen and subsequent response times to assess their effects with the semi-quantitative methods. However, in real plants, process operation conditions such as pressure, temperature, and flow rate can vary from the steady-state conditions when the process is in a transient state due to its shut-down or set point changing operation. During these operation procedures, process operating variables are unlikely to decrease or increase monotonously due

to the interaction of convolutedly connected process units, which might result in higher pressure or temperature or flow rate points than those of steady-state values, finally posing a greater risk. In this point of view, dynamic simulations can serve as a tool to detect these blind spots which are hidden in steady-state simulations and to discover underestimated risks. In summary, they allow to design more reliable safety systems by revealing the potential risks that cannot be detected under steady-state conditions.

In this section, a QRA integrated with a dynamic simulation and an accident simulation is conducted to discover the blind spots during a normal operation for the target process of heavy oil desulfurization (HOD), which is currently installed and being operated in Seosan city, South Korea. A new QRA methodology for integration of dynamic process modeling and accident modeling is proposed with commercial software of Aspen HYSYS V10 and SAFETI V8.22. First, a dynamic model of shut-down procedure is constructed by Aspen HYSYS V10 and the trends of process variables are observed. After identifying the maximum pressure points through dynamic simulation, those are used as inputs for risk evaluation by SAFETI V8.22. Among the various subsections in the HOD process, the reactor section is selected for risk calculations for its high likelihood of risks occurrence judging by the highest operating conditions of the temperature and pressure.

In section 2.3, the QRA methodology is outlined through the integration of dynamic process simulation and accident simulation. In section 2.4, the target process is introduced and inputs of the QRA are estimated by the hazard identification consequence and frequency analysis in the way of suggested

methodology. In section 2.5, the outcome is compared with the conventional QRA result and these two cases are analyzed to see how much the newly discovered blind spots have an impact on the risk calculation results. Finally, the process is judged to be intolerable and an additional mitigation procedure is proposed.

2.3. Methodology

2.3.1. General sequence of QRA

The QRA is a formal and systematic risk analysis approach to quantifying the risks associated with the operation of an engineering process. Figure 2-1 shows the conventional and general six-step QRA procedure which is widely used in many studies over the world. [20] [21] [22] [23] After determining the domain of the target process to be analyzed in a QRA, hazards such as discharge, dispersion, fire, and explosion are identified by several methods, e.g., HAZOP, then their consequence and frequency are analyzed respectively. Mostly, consequences are estimated by commercial software which can compute one-dimensional parametric models or multi-dimensional models and Frequencies are acquired from historical data such as Oil and Gas Producers (OGP) [24]. Once the consequence and frequency analyses are finished, they are summed up and the results are used as criteria to determine whether the system domain is acceptably safe. For the processes that turned out to have intolerable risks, additional risk mitigation procedures such as process design modification or mounting of safety barriers are required.

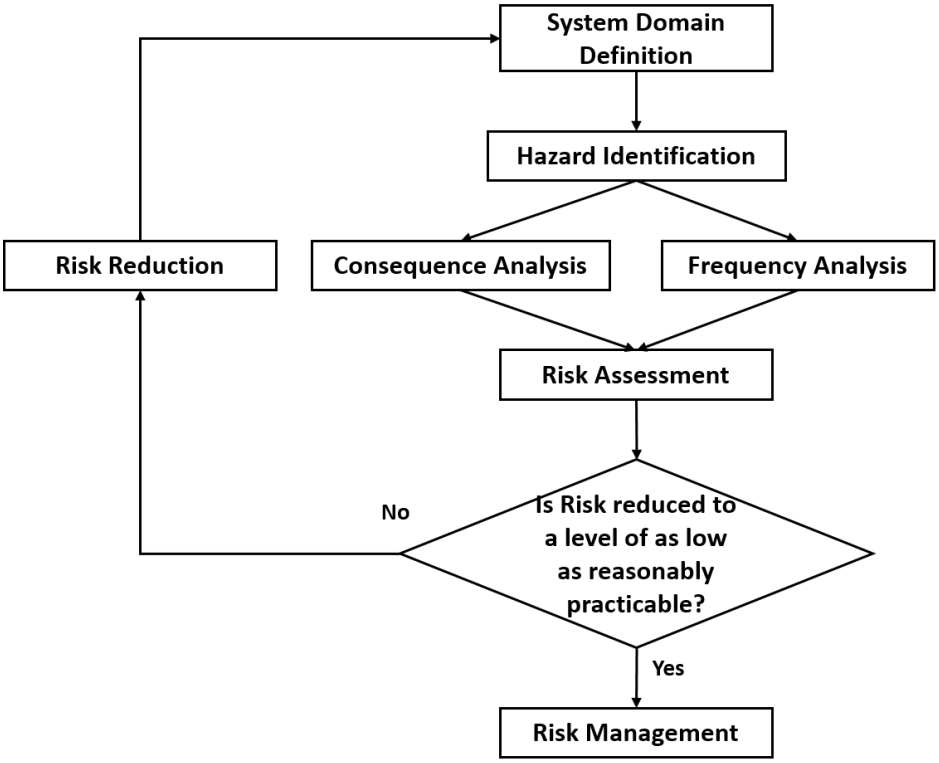

Figure 2-1. Conventional procedure of QRA

Two criteria are available when judging the risk tolerability: Individual Risk (IR) and Societal Risk (SR). IR is the annual risk of death or serious injury to which an individual are exposed at the same location, whereas SR is the risk of health consequences related to the population that may be affected by hazardous incidents in a certain region. Since IR cannot reflect the overall risk of different plants with a variety of population density, SR is more widely used. The most representative method to show SR is to plot F-N curve, where F indicates the frequency of the N number of fatalities occurrence. In this study, F-N curve method is adopted as the standard for the tolerability criterion.

2.3.2. QRA with dynamic simulation of shut-down procedure

As described earlier, dynamic simulation allows to reveal the blind spots that would be unable to be found by the steady-state simulation. To verify this claim, a shut-down procedure is simulated by Aspen HYSYS V10 with a combination of HAZOP analysis results prepared by the license company. As the shut-down procedure proceeds, controllers and corresponding actuators, e.g., valves, operate sequentially, resulting in changes of process variables such as temperature, pressure and flow rate. However, process variables would not simply decrease monotonously, but show complex behavior due to the non-linear interaction of multiple controller logic over the process. Thus, although the operating condition becomes in the rest state of processes eventually, it can get harsher during the shut-down procedure than the normal operating condition. If the increased risks caused by the harsher condition were ignored for performing QRA, the risk of the process would be underestimated and accidental events would result in disastrous damages. For this reason, in this study, the highest values of the operating conditions are utilized as inputs to conservatively assess the risk. Using the obtained simulation results, accident simulations are conducted with SAFETI V8.22. Damages such as thermal radiation and consequent lethality are evaluated by the built-in models based on the storage conditions (temperature, pressure, mixture property, and mass inventory) of individual process units such as vessels or pipelines. The remaining steps of the QRA follows the conventional method which are specified in section 2.3.1. The structure of the proposed QRA methodology is shown in Figure 2-2.

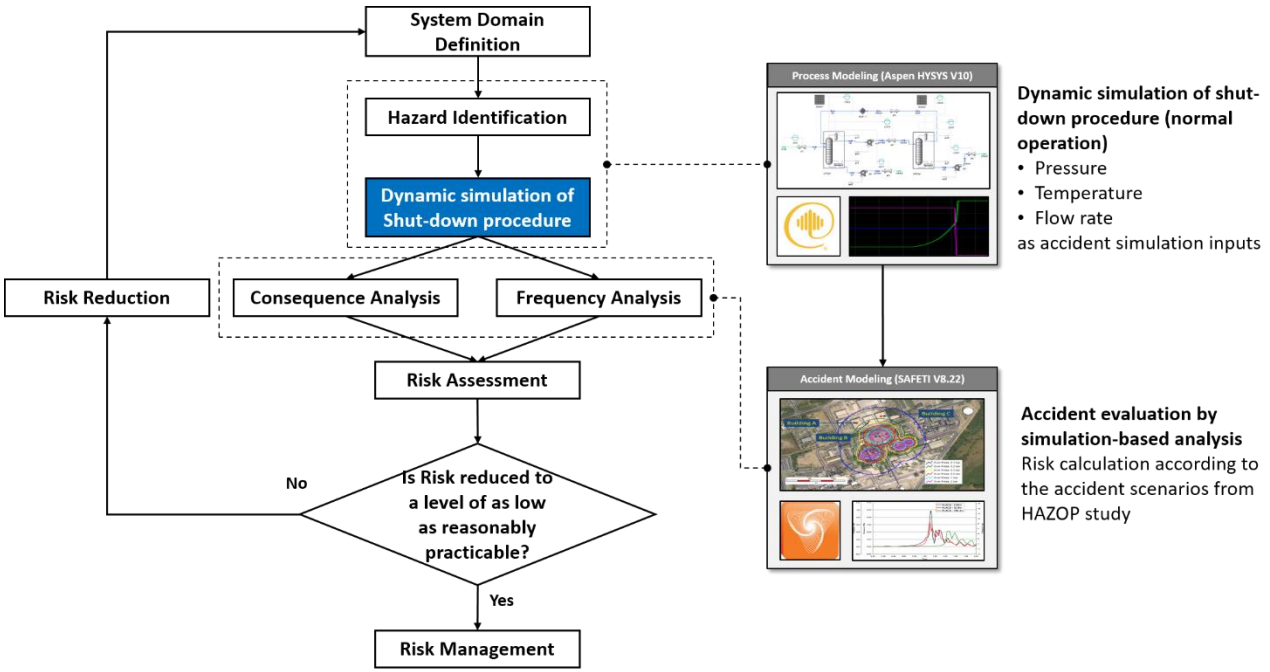

Figure 2-2. Schematic of proposed QRA methodology

2.4. Implementation of QRA for reactor section in HOD process

2.4.1. Target process description: Reactor section in HOD process

The overall configuration of the HOD process is introduced in section 1.2. As can be seen in Figure 1-1, the reaction occurs under high pressure and temperature conditions, and is exothermic, making the product stream have high temperature. The process flow diagram of the reactor section is shown in Figure 2-3. The feed of high sulfur atmospheric residue from the distillation unit is routed to feed pump to meet the reaction condition of 200 barg. Then, the pressurized stream is heated by the higher temperature reactor effluent to meet the other reaction condition of 350 ℃. Finally, after obtaining additional heat from the feed furnace, the reaction proceeds through the five reactors in series. Keeping the reaction conditions of temperature and pressure constant is the key to the chemical equilibrium and the consequent yield. To achieve this goal, the feed flow rate is controlled by the flow rate controller 1 (FC1 in Figure 2-3) and the pressurized feed by the feed pump is controlled by the pressure controller 1 (PC1 in Figure 2-3). The inter-reactor streams are controlled by adjusting the flow rate of quench gas lines, which are kept constant by the flow rate controller 2-5 (FC2-5 in Figure 2-3) and temperature of the reactor outlet stream which goes to the separation section is controlled by manipulating the flow rate of the reactor inlet side stream which is kept constant by the temperature controller 1. (TC1 in Figure 2-3) This process undergoes periodical

shut-downs and start-ups to change catalysts which are located in the reactors. The controllers and their related actuators (in this case, values) allow the process variables to be changed smoothly during the periodical shut-down and start-up operations.

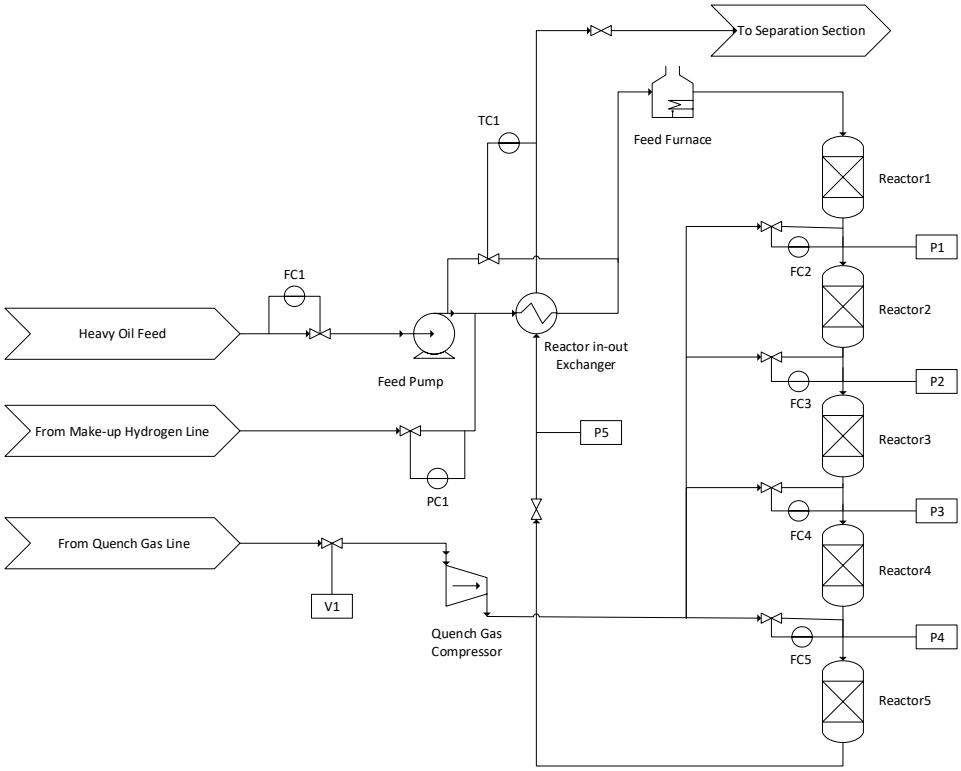

Figure 2-3. Process flow diagram of reactor section of HOD process

The HOD process model is constructed by Aspen HYSYS V10 and the required data for dynamic simulation such as the size of each equipment is obtained from the corresponding piping and instrument diagram (P&ID) of HYUNDAI Oil Bank company. The plot plan which depicts the layout of the process units for the target process is shown in Figure 2-4, which is blurred due to confidentiality. The area marked with a rectangle at the bottom left is the reactor section.

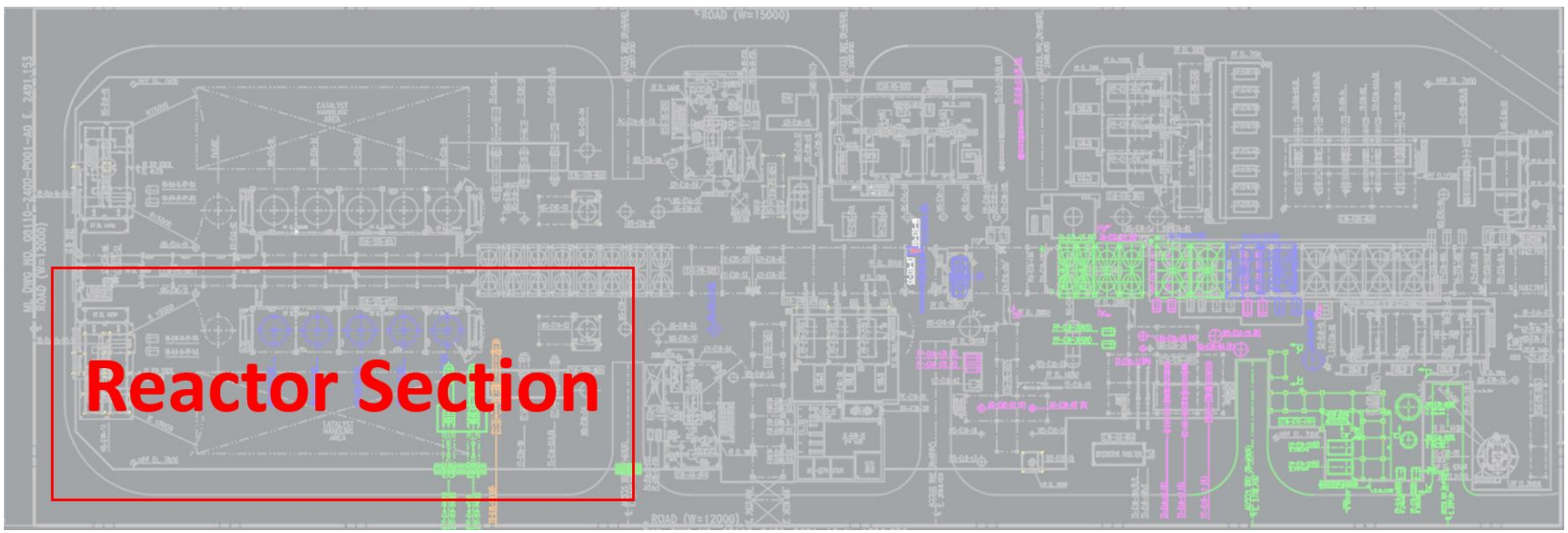

Figure 2-4. Plot plan of HOD process

2.4.2. Hazard identification and dynamic simulation of shut-down procedure

Hazard identification is the process to evaluate if any particular situation, item, etc. may have the potential to cause harm. According to the HAZOP report of the license company, due to the harsh operating conditions of the reactors, release accidents through the pipeline flanges near the reactor are most likely to happen. For this reason, pipelines of P1-5 located close to the reactors, of which the operating pressures and temperatures lie in the range of 175-195 barg and 380-390°C, respectively at a normal operation are chosen as hazards. The locations of P1-5 can be identified in Figure 2-3, and individual unit descriptions and operating conditions are specified in Table 2-1.

Table 2-1. Unit description and steady-state operating conditions of hazard points

Unit	Description	Pressure (barg)	Temperature (℃)	Flow (10^4 kg/h)
P1	Piping from reactor_1 to reactor_2	192.4	388.1	2.381
P2	Piping from reactor_2 to reactor_3	191.6	385.4	2.403
P3	Piping from reactor_3 to reactor_4	186.4	382.7	2.435
P4	Piping from reactor_4 to reactor_5	181.1	381.8	2.473
P5	Piping from reactor_5 to reactor in-out exchanger	175.6	380.2	2.494

To discover potential blind spots, a normal operation of shut-down procedure is simulated according to the operation manual. The entire shut-down procedure of the HOD process takes around three hours. However, in the reactor section all procedures are completed within one hour and most of the process variables are stabilized. Therefore, in this paper, only the first one hour of the shut-down procedure is analyzed and the details are as follows:

I. The heavy oil feed line is closed by converting the operation mode of FC1 to manual state and closing the corresponding actuator.
II. Quench gas line V1 is closed to start depressurization of the reactors followed by converting the operation mode of FC2-5 to manual state and closing the corresponding actuators sequentially.
III. The fuel supply to the feed furnace is cut off to decrease the temperature of the process.
IV. The make-up hydrogen line is closed by converting the operation mode of PC1 to manual state to further stabilize the pressure of the process.
V. To keep the temperature of the product line to separation section decreasing, the operation mode of TC1 is converted to the manual state.

According to the shut-down sequence described above, dynamic process simulation is performed with Aspen HYSYS V10 with the modified Peng-Robinson equation of state model [25]. Figure 2-5 shows the dynamic simulation results of the pipelines P1-5 during the shut-down procedure.

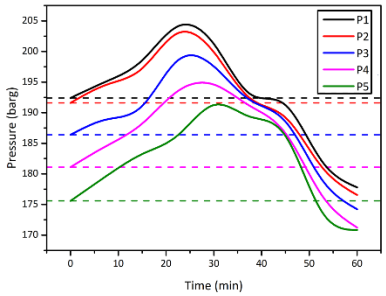

(a) Pressure trend

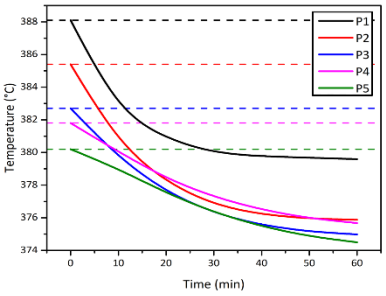

(b) Temperature trend

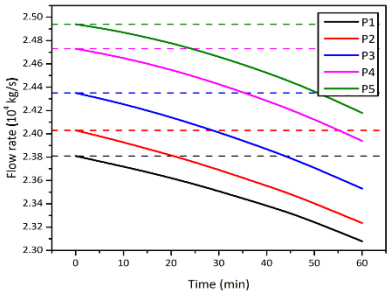

(c) Flow rate trend

Figure 2-5. Trend of process variables for first one hour during shut-down process

In Figure 2-5(b) and 2-5(c), it can be checked that the temperature and flow rate of P1-5 decrease over time from the beginning of the shutdown procedure. However, in Figure 2-5(a), contrary to what might be thought intuitively, the pressure values increase even higher than those of the steady-state operation and when the pressure values reach certain points, they start to decrease until the shutdown is over. The cause of this phenomenon can be surmised by analyzing the shutdown procedure, specifically the procedure II. The isolation of quench gas line begins with the closing of V1 first, which reduces the flow rate entering the quench gas compressor. As V1 closes faster than cutting off the electric work supplied to the quench gas compressor, the pressure of the streams entering the reactors through the actuators FC2-5 increases, which leads to the temporary increase of the reactor pressure.

2.4.3. Consequence analysis

In the case of release scenario, accident consequences are determined by temperature, pressure, flowrate, and physical properties of the materials used in the process. To estimate the consequence, calculations of released fluid concentration along with the downwind distance should be conducted using the inputs of operating conditions such as temperature, pressure, flow rate, and composition, of which values can be obtained from dynamic simulation of the HOD model operating according to the shutdown procedure. In general, the most significant input variable that affects outcomes of an accident is pressure. Although the tendency of decrease in temperatures and flow rates are identified, the damage might be more severe due to the increase of pressures. Thus, the consequence of risks with these newly found input variables should be calculated to confirm the change of the outcome. To achieve this goal, the maximum pressure values for the curves of each of P1-5 in Figure 2-5(a) are selected as input variables to postulate the worst case. In addition, the temperature values at the time of each maximum pressure observed are obtained as other input variables from Figure 2-5(b). The consequence is calculated for each process equipment (in this case, pipelines), which requires the static storage conditions as the input variables. However, as the process model is constructed using flow-based calculations, the operating conditions obtained from simulation should be converted to the static inventory conditions using the following equation.

$$I = \rho_f V + kM \tag{2-1}$$

Where $\rho_f, V, k,$ and M represent mass density of hold-up fluid, hold-up volume in process equipment, release duration, and mass flow rate respectively. In an actual site, the isolation of the relevant line is completed in ten minutes in case of a release. Therefore, a ten-minute release duration is assumed for the sake of conservative risk assessment and the static inventory is calculated by summing up the flow rates for ten minutes from the maximum pressure points. The input values are shown in Table 2-2 and simulations were performed to assess the risk consequence of the shut-down process. Also, additional simulations were performed with the steady-state conditions of Table 2-1 to compare the suggested methodology with the conventional one.

Table 2-2. Risk calculation input values from dynamic simulation conditions

Unit	Time (min)	Pressure (barg)	Temperature (°C)	Mass inventory (10^3 kg)
P1	22.4	204.1	380.9	3.831
P2	22.5	202.9	378.3	3.966
P3	26.0	198.5	376.3	4.033
P4	29.8	194.5	376.5	4.081
P5	31.2	191.2	375.5	4.168

2.4.4. Frequency analysis

Having identified hazards which are likely to cause severe damages to the process, the final step is to estimate the probability of each hazard occurrence. First of all, the event tree analysis (ETA) which is a forward and top-down modeling technique is performed to identify the entire possible outcomes. The ETA structure shown in Figure 2-6 provides a variety of outcomes, encompassing immediate ignition, delayed ignition, short-duration release, etc. Probabilities for the consequences of the right end in the event tree are determined by the probabilities of each intermediate node, which is generally obtained from historical records of how often a specific event of each node occurred. In this study, the release frequencies of the pipelines are determined from OGP 2010 [24]. The ignition probabilities were estimated from release rates calculated by the SAFETI V8.22 discharge model and look-up correlation which consists of three gradients based on release rate and release scenario. [26] The default value of 0.3, widely used for normal on-site processes was used as the immediate ignition probabilities and the moderate value of 0.2 for a major release rate (1-1000 kg/s) is used as the explosion probabilities. Table 2-3 shows the probabilities of each node in the event tree, which were evaluated using the steady-state conditions as the base case and Table 2-4 shows those of the dynamic simulation conditions.

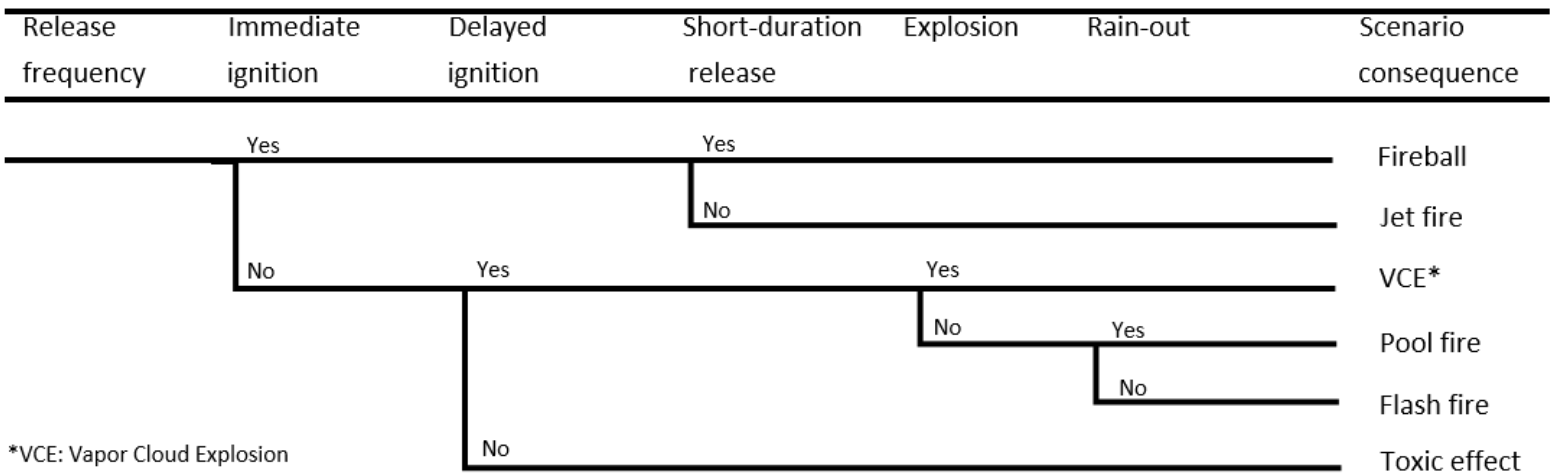

Figure 2-6. ETA structure of HOD process

Table 2-3. Probabilities of each node of ETA in steady-state simulation conditions

Release scenario	Release rate (kg/s)	Release frequency	Ignition probability
P1_10mm	3.17×10^{0}	3.9×10^{-5}	9.10×10^{-3}
P1_50mm	7.94×10^{1}	1.6×10^{-5}	1.38×10^{-1}
P1_150mm	7.15×10^{2}	3.2×10^{-6}	6.51×10^{-1}
P2_10mm	3.16×10^{0}	3.9×10^{-5}	9.01×10^{-3}
P2_50mm	7.94×10^{1}	1.6×10^{-5}	1.31×10^{-1}
P2_150mm	7.14×10^{2}	3.2×10^{-6}	6.35×10^{-1}
P3_10mm	3.10×10^{0}	3.9×10^{-5}	8.94×10^{-3}
P3_50mm	$7{,}76 \times 10^{1}$	1.6×10^{-5}	1.21×10^{-1}
P3_150mm	6.98×10^{2}	3.2×10^{-6}	6.19×10^{-1}
P4_10mm	3.02×10^{0}	3.9×10^{-5}	8.79×10^{-3}
P4_50mm	7.55×10^{1}	1.6×10^{-5}	1.17×10^{-1}
P4_150mm	6.79×10^{2}	3.2×10^{-6}	6.03×10^{-1}
P5_10mm	2.92×10^{0}	5.1×10^{-5}	8.78×10^{-3}
P5_50mm	7.31×10^{1}	2.1×10^{-5}	1.10×10^{-1}
P5_150mm	6.58×10^{2}	4.1×10^{-6}	5.95×10^{-1}

Table 2-4. Probabilities of each node of ETA in dynamic simulation conditions

Release scenario	Release rate (kg/s)	Release frequency	Ignition probability
P1_10mm	3.37×10^{0}	3.9×10^{-5}	9.12×10^{-3}
P1_50mm	8.44×10^{1}	1.6×10^{-5}	1.40×10^{-1}
P1_150mm	7.60×10^{2}	3.2×10^{-6}	6.55×10^{-1}
P2_10mm	3.37×10^{0}	3.9×10^{-5}	9.03×10^{-3}
P2_50mm	8.43×10^{1}	1.6×10^{-5}	1.33×10^{-1}
P2_150mm	7.58×10^{2}	3.2×10^{-6}	6.39×10^{-1}
P3_10mm	3.31×10^{0}	3.9×10^{-5}	8.95×10^{-3}
P3_50mm	8.27×10^{1}	1.6×10^{-5}	1.25×10^{-1}
P3_150mm	7.45×10^{2}	3.2×10^{-6}	6.22×10^{-1}
P4_10mm	3.21×10^{0}	3.9×10^{-5}	8.81×10^{-3}
P4_50mm	8.11×10^{1}	1.6×10^{-5}	1.18×10^{-1}
P4_150mm	7.30×10^{2}	3.2×10^{-6}	6.07×10^{-1}
P5_10mm	3.18×10^{0}	5.1×10^{-5}	8.70×10^{-3}
P5_50mm	8.03×10^{1}	2.1×10^{-5}	1.12×10^{-1}
P5_150mm	7.18×10^{2}	4.1×10^{-6}	5.98×10^{-1}

2.5. Results and discussion

2.5.1. Implementation of QRA by commercial software and analysis of the results

Summing up all of the data in the previous sections, risks can be assessed quantitatively by SAFETI V 8.22, which is widely used commercial software in release, dispersion, fire and explosion simulations. The additional input data such as population density and weather conditions are obtained from the license company. According to Health and Safety Executive (HSE)'s report [27], an individual risk of less than 1.0×10^{-6} per year is considered negligible, while it is intolerable above 1.0×10^{-4} per year for the public and above 1.0×10^{-3} per year for workers on the site. The region between these two criteria, negligible and intolerable, is called as low as reasonably practicable (ALARP) and the upper ALARP limit, 1.0×10^{-3} per year is generally used to judge whether a process is tolerable or not. As above-mentioned criteria, two risk calculation results with different process variables as inputs are compared and analyzed, one is performed with the steady-state conditions (STD case) in Table 2-1 and 2-3, and the other is performed with the dynamic simulation conditions (DYN case) in Table 2-2 and 2-4.

The IR contours on the plot plan of the reactor section of the DYN case and the STD case are shown in Figure 2-7, the contours are calculated from Equation 4 and Equation 5 as below:

$$IR_{x,y} = \sum_{i=1}^{N} IR_{x,y,i} \quad (2\text{-}2)$$

$$IR_{x,y,i} = F_i \times P_{fi} \quad (2\text{-}3)$$

Where subscripts x and y represents the position, and i denotes the event. As can be seen in Figure 2-7, although the DYN case used smaller input values of temperature and mass inventory than the STD case, the overall damage of the DYN case is bigger than that of the STD case due to the higher pressure values. This confirms the general tendency that pressure affects accident results more than temperature or flow rate is also applied to the reactor section of the HOD process. In both cases, significant amounts of the process are located outside the red (1×10^{-5} : lower ALARP limit) curve. However, this does not reflect the reality because the curves just show annual damages that a person undergoes who is standing at the same location for one year, without taking into account any population density. Therefore, in order to quantitatively assess the risks considering the population density, F-N curves for the SR are plotted in Figure 2-8. In the STD case, the total risk (Total $risk_{STD}$) which is the summation of flammable effects (Flammable $risk_{STD}$) and toxic effects (Toxic $risk_{STD}$) of all accident scenarios is found not to exceed the MAX. ALARP line, while in the DYN case, the total risk (Total $risk_{DYN}$) which is the summation of flammable effects (Flammable $risk_{DYN}$) and toxic effects (Toxic $risk_{DYN}$) of all accident scenarios is found to exceed the MAX. ALARP line from 2.7 to 6.3 fatalities. As a result, the risk of the DYN case is judged to be intolerable and additional mitigation procedures are necessary to pull the Total $risk_{DYN}$ curve down below the MAX. ALARP line. In both F-N curves, the flammable effect is dominant over the toxic effect due to the relatively small amount of hydrogen sulfide which is the sole trigger of the toxic effect in the HOD process. Therefore, when performing a risk reduction procedure in the DYN

process, scenarios that cause flammable effects should be mitigated preferentially.

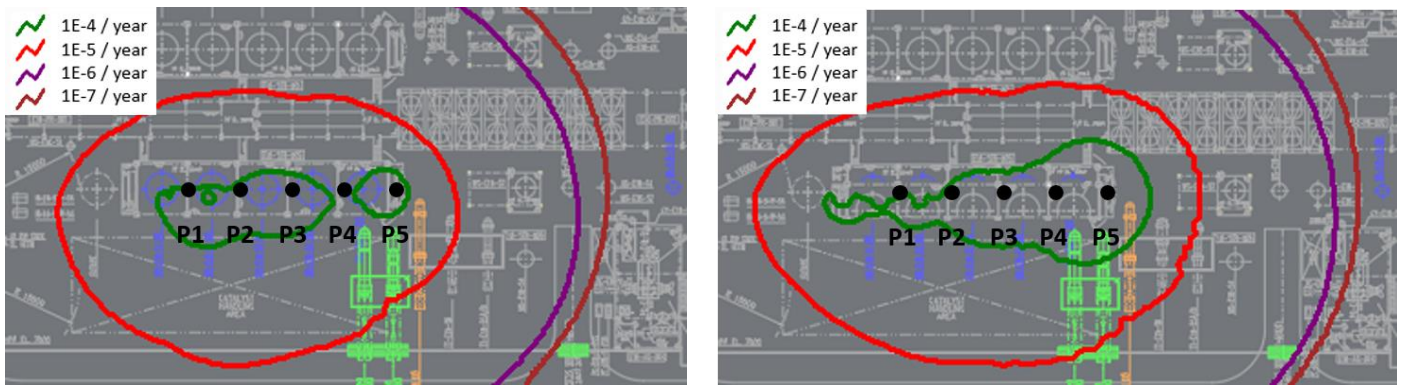

(a) Individual risk contour (STD case) **(b) Individual risk contour (DYN case)**

Figure 2-7. Individual risk contours for STD case and DYN case

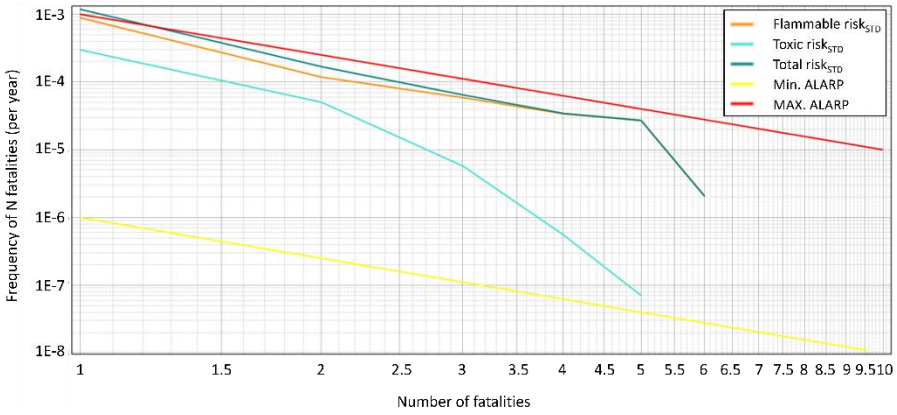

(a) F-N curve (STD case)

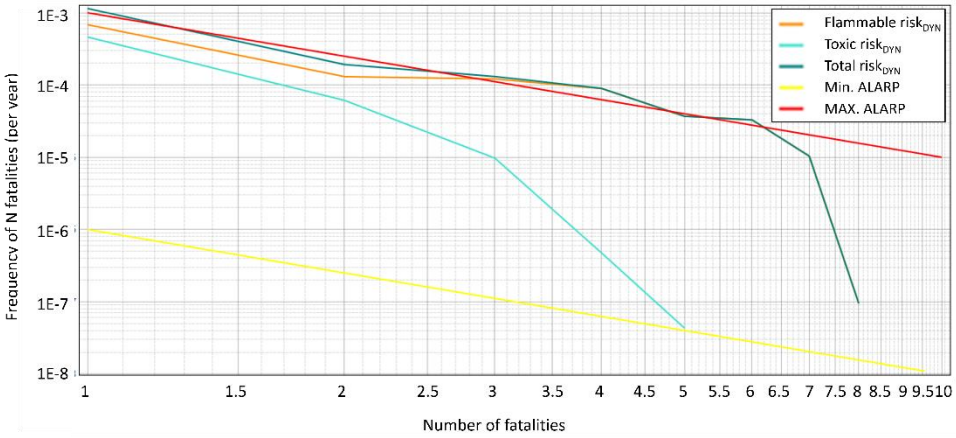

(b) F-N curve (DYN case)

Figure 2-8. F-N curve for STD case and DYN case

Before performing a risk reduction procedure, it is worthwhile to quantitatively analyze how the pressure of P1-5 increased in the DYN case. For the analysis, changes of flammable risk integrals in STD case and the DYN case are shown in Table 2-5 and the summations of risk integrals of each unit (P1-5) for Table 5 are shown in Figure 2-9. It can be check that the overall risk integral of the DYN case increases by 8% and each of P1-5 increases around 10% compared to the STD case. Referring to Table 2-1 and Table 2-2, the P5 has the highest rate of pressure increase, resulting in the highest rate of risk integral, as can be seen in Figure 2-9. The increased pressure can affect the risk outcomes in two ways: consequence and frequency. When SAFETI V8.22 evaluate the consequence, the discharge model first calculates release rate based on the pressure difference between the vessel and atmosphere at the orifice. Afterwards, dispersion, pool fire, jet fire, explosion, and other accident scenarios are calculated subsequently. Since these scenarios are all affected by the discharge result at first, the change in the result of discharge due to the pressure change influences all the outcomes of the accident scenarios. Additionally, the ignition probabilities in the ETA is also affected as can be identified in Table 2-3 and Table 2-4 since those values are computed by look-up correlation based on the release rate. [26] Therefore, increase in pressure inputs results in the increase of both consequence and frequency, which has a large impact on the risk integral

(risk outcome). For this reason, even if the temperature and flow rate decreases, the risk integral is likely to increase when considering dynamics of the shut-down process.

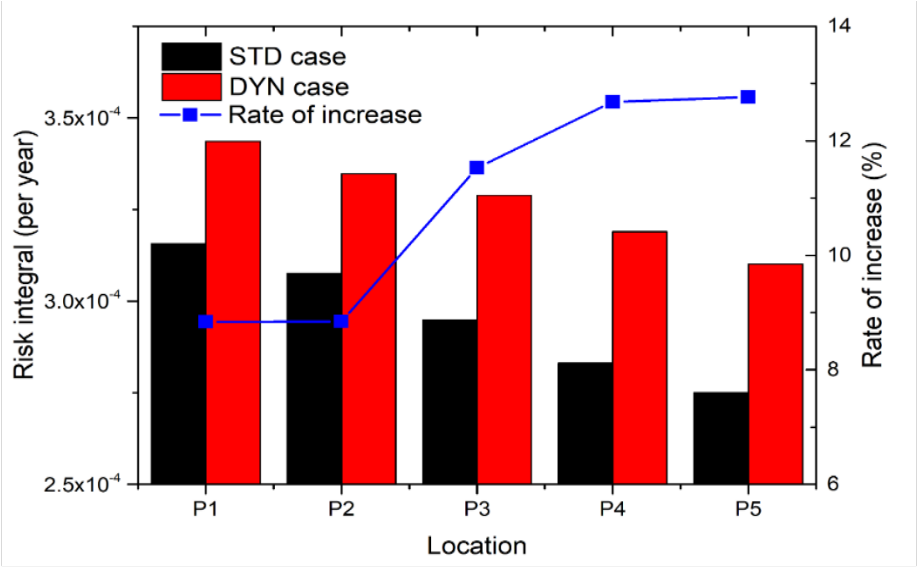

Figure 2-9. Unit-wise integral summation and rate of increase from STD case to DYN case

Table 2-5. Flammable risk integrals of STD case and DYN case

Release scenario	Risk integral of STD case (per year)	Risk integral of DYN case (per year)	Rate of increase (%)
P1_10mm	7.37×10^{-5}	7.86×10^{-5}	6.73
P1_50mm	1.17×10^{-4}	1.27×10^{-4}	8.74
P1_150mm	1.25×10^{-4}	1.38×10^{-4}	9.92
P2_10mm	7.16×10^{-5}	7.68×10^{-5}	7.19
P2_50mm	1.14×10^{-4}	1.24×10^{-4}	9.21
P2_150mm	1.22×10^{-4}	1.34×10^{-4}	10.40
P3_10mm	6.89×10^{-5}	7.49×10^{-5}	8.76
P3_50mm	1.09×10^{-4}	1.21×10^{-4}	10.81
P3_150mm	1.17×10^{-4}	1.33×10^{-4}	12.02
P4_10mm	6.61×10^{-5}	7.30×10^{-5}	10.46
P4_50mm	1.05×10^{-4}	1.18×10^{-4}	12.54
P4_150mm	1.12×10^{-4}	1.28×10^{-4}	13.77
P5_10mm	6.40×10^{-5}	7.11×10^{-5}	11.10
P5_50mm	1.02×10^{-4}	1.15×10^{-4}	13.19
P5_150mm	1.09×10^{-4}	1.24×10^{-4}	14.42
Total	1.48×10^{-3}	1.64×10^{-3}	10.81

To further analyze the outcome, the major outcomes of the P5_150mm scenario which has the highest increase rate of risk integral are listed in Table 2-6. In both of the STD case and the DYN case, the continuous release with rainout immediate horizontal jet fire with additional pool fire effect (CRIHJP) is dominant over the summation other scenarios by a factor of ten to one hundred. When leaking through an orifice (hole) to atmospheric temperature and pressure conditions, the fluid at high temperature and high pressure conditions undergoes a two-phase release (gas and liquid) and the gas expands to a large extent with a great amount of momentum, leading to the magnificent impact of jet fire than other accident scenarios. Part of these scenarios are shown in Figure 2-10 and Table 2-7, in which the increments of lethality radius in jet fire and flash fire scenarios are identified

Table 2-6. Major outcomes of P5_150mm release scenario

P5_150mm release scenario	Risk integral of STD case (per year)	Risk integral of DYN case (per year)	Rate of increase (%)
CRIHJP[a]	9.11×10^{-5}	1.06×10^{-4}	16.72
CRDRPF[b]	1.05×10^{-5}	1.07×10^{-5}	1.66
CRDFFP[c]	3.11×10^{-6}	3.14×10^{-6}	1.03
CRDFXP[d]	3.09×10^{-6}	3.22×10^{-6}	4.24
Total	1.07×10^{-4}	1.23×10^{-4}	14.42

[a]Continuous release with rainout immediate horizontal jet fire with additional pool fire effect

[b]Continuous release with rainout delayed residual pool fire

[c]Continuous release with rainout delayed flash fire with pool fire

[d]Continuous release with rainout delayed flash fire with explosion and pool fire

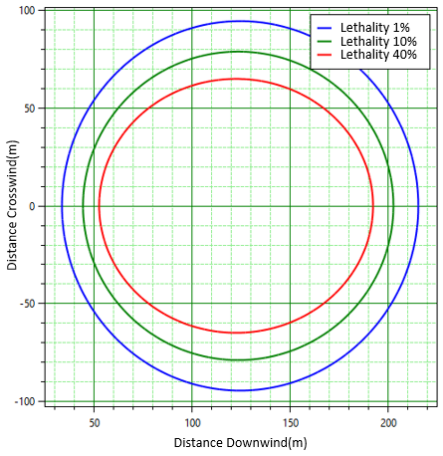

(a) Lethality radius of jet fire for STD case

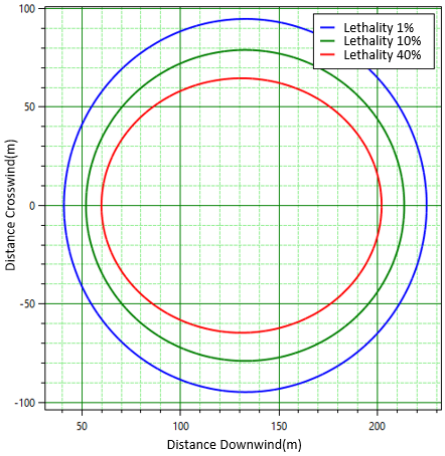

(b) Lethality radius of jet fire for DYN case

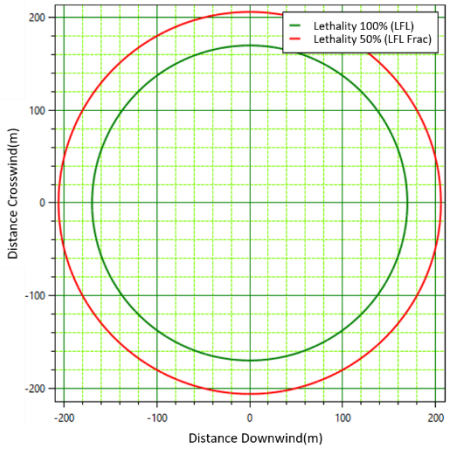

(c) Lethality radius of flash fire for STD case

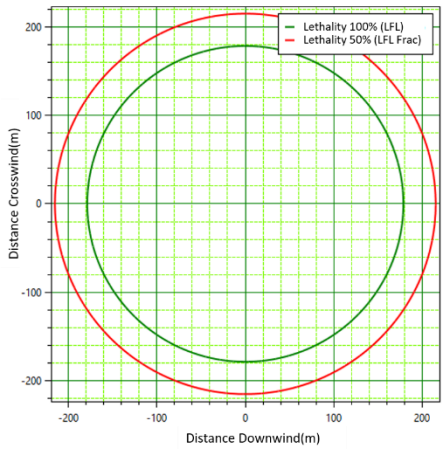

(d) Lethality radius of flash fire for DYN case

Figure 2-10. Consequence of P5_150mm for STD case and DYN case

Table 2-7. Consequences of P5_150mm for STD case and DYN case

		STD case (175.6 barg)	DYN case (191.2 barg)
Scenario	Lethality (%)	Distance downwind (m)	
Jet fire	40	191	202
	10	202	212
	1	215	222
Scenario	Lethality (%)	Distance downwind (m)	
Flash fire	100 (LFL)	170	180
	50 (LFL Frac)	204	216

2.5.2. Risk reduction

As the DYN case are judged to be intolerable, risks should be reduced by dragging down the F-N curve below the MAX. ALARP line. The most fundamental solution is to change the sequence of shut-down procedure. However, in this case, the reactor section is connected to other sections such as fractionation section, recycle gas compression section, etc. Therefore, changing the sequence of shut-down procedure in reactor section signifies changing the sequence of shut-down procedure in the entire HOD process as the dynamics of a certain section affects that of other sections, which means the risk of the entire HOD process should be re-assessed accordingly. Since the methodologies of risk reduction are not standardized, one or more options are available. The one is to modify the overall layout by repositioning the process units. This is usually implemented by giving greater separation distances, preventing hazards from overlapping. Another way is to change the operating conditions to reduce the consequence and frequency of accident scenarios. However, these solutions are difficult to be applied considering the huge amount of cost required for modifying the process already in operation and the loss of profit for the meanwhile.

Other feasible option for mitigating risks is to install safety barriers to reduce both consequence and frequency. Safety instrumented systems can be applied with an advanced logic of process controllers or fire walls can also be installed to mitigate the physical damage of accidents. Since the risk integral value of CRIHJP scenario is dominant over the other scenarios as in Table 6, safety barriers which can mitigate

the effect of jet fires should be considered preferentially. Moreover, as the risk integrals are evenly distributed over P1-5, installation of safety barriers should not concentrate on a specific reactor, rather it should cover the whole reactor section. As an initial safety action, installing fire walls around the reactors which reduce the damages of the consequence is adopted as the risk mitigation method and the result is shown in Figure 2-11(a). The majority of F-N curve is pulled down but still the points near 4 fatalities are above the MAX. ALARP line due to the vast impact of jet fires on the consequence. For this reason, as an additional safety barrier, sensors that can detect leakages over the whole process in the early stage of accidents are considered to be installed, which can be expected that the release frequencies substantially decrease by a factor of ten [28]. The result is shown in Figure 2-11(b), in which the total risk curve is pulled down below the MAX. ALARP line and consequently, a safer and more reliable operation of the reactor section in the HOD process is accomplished.

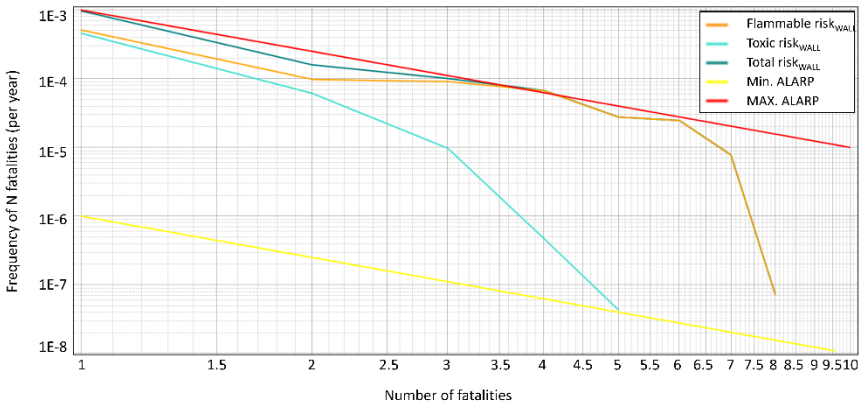

(a) F-N curve after installing fire walls

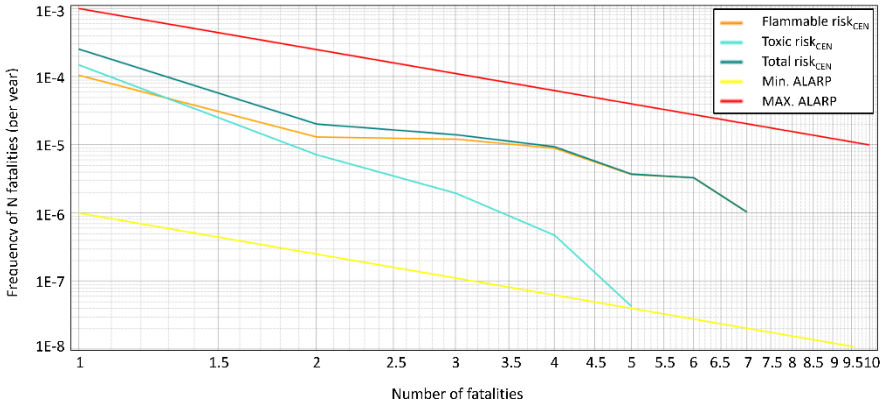

(b) F-N curve after deploying additional sensors

Figure 2-11. F-N curves after mitigation

2.6. Conclusion

In this paper, a dynamic process simulation of the reactor section in the HOD process and a subsequent QRA was implemented to identify potential risks which are undetectable by the conventional method. First, potential hazards were estimated qualitatively near the reactor which have high operation pressure and temperature conditions, thus are likely to be susceptible to release accidents. In the next step, a dynamic process simulation was conducted to identify potential hazards quantitatively during a shut-down process. Several points were found to be more dangerous than the steady-state, and a QRA was performed using those values of newly detected points. An additional QRA was carried out using the process variable values of the steady point, which is the general QRA method, to compare the result of the proposed methodology with the conventional one.

As a result, the QRA outcome with the dynamic simulation conditions was judged to be intolerable as the F-N curve exceed the MAX. ALARP line, while the QRA outcome with the steady-state conditions was judged to be tolerable. The result of those two cases were compared for analysis, where the newly discovered points in the dynamic process simulation had lower temperatures and flow rates than the steady-state but higher pressures, resulting in an overall risk integral elevation of 11% with increases of risk integrals for the individual process units (P1-5) by about 6-14%. The jet release and subsequent jet fire scenarios were found to have the largest impact on the consequence because the released materials which undergo a drastic expansion from the high operating conditions to the atmospheric conditions

obtain a great amount of momentum. Finally, a mitigation procedure to drag down the F-N curve which was judged to be intolerable below the MAX. ALARP line was carried out and a reliable operation of the reactor section in the HOD process became possible.

Through the QRA integrated with dynamic process behavior and accident outcomes, the blind spots which would have been undetectable in the steady-state were found and proper actions could be taken accordingly. As confirmed in this study, risks could exist not only in malfunction of process units but in normal operations such as the shut-down procedure, in which process variables can fluctuate drastically and result in a huge variation from the values of the steady-state. Therefore, it is worthwhile to confirm dynamic process behavior of a process through a dynamic simulation, to capture the inherent risks which are hidden in the steady-state and the appropriate action to additionally identified risks will greatly contribute to a more reliable and trustable process operation.

Chapter 3. Plant-wide dynamic simulation with 3D accident simulation: Development of operator training system

3.1. Introduction

While the growth of chemical engineering industry has given birth to a number of profits, the increased risk due to the expansion of process size and complexity is another concern for chemical engineers. Today, since processes are becoming more compact and dense, the damage becomes even higher. For example, the catastrophic explosion on March 23, 2005 at the British Petroleum (BP) refinery in Texas brought about 195 casualties. [29] According to the investigation report, inadequate training for operations personnel, particularly for the board operator position, contributed to causing the incident. In other researches, it is also identified that the main cause of accidents which occur in plants is mal-operation of process equipment by operators due to the lack of previous education [30], followed by insufficient knowledge about the process [31], and finally resulting in a number of man-made disasters.

For a long time, many people and organizations who recognized this problem have worked hard to prevent accidents. They mainly have focused on educating and training operators in order for them to take actions in case of emergency situations, expecting to reduce physical and economical damage. This movement have promoted the expansion of the operator training system (OTS) market [32], and

there has been a notable progress in this area. OTS is mainly based on dynamic process simulation [33] [34] [35]like UniSim® by Honeywell and Aspen® by AspenTech. The education usually start from the upsets of process variables such as pressure, temperature and flow rate around certain process units such as compressors, reactors, etc. Once these abnormal situations happen, OTSs induce the trainees to take proper actions such as closing the valves in sequence or shutting down the relevant process units. In this manner, OTSs have contributed a lot to educating control room operators (CROPs) on what to do when an emergency occurs. However, these kinds of process-simulation-based OTS have limitations in educating field operators (FOPs) because accident situations such as leak, fire and explosion cannot be included in training scenarios.

3.2. Background

Since close cooperation between CROPs and field operators (FOPs) is essential in the field [36], there have been attempts to combine accident simulation results such as toxic gas concentration, thermal radiation, overpressure and even virtual reality (VR) with OTSs to educate both CROPs and FOPs by sharing process and accident information. Cha et al. [37] developed a fire case training program in the VR, which compute fire effect using computational fluid dynamics. Schneider Electric [38] tried mapping a visual effect of fire onto the VR using the platform of EYESIM® in which process structures are realized with the aid of process simulation. Even though above-mentioned two attempted to resolve the conventional integration problem, they failed to directly connect process simulation with accident simulation. To resolve this, Manca et al. [39] proposed a solution of augmented virtual reality (AVR) of Virthualis in which additional process information such as trends of pressure, temperature and flow rate is imposed in the virtual environment by integrating the process simulator of UniSim® with the self-developed accident simulator of AXIM. They made use of object linking and embedding (OLE) technology to effectively connect these two modules and finally mapped a two-dimensional pool fire simulation result to the VR in real time, consequently constructing the AVR. This methodology computes simple parametric two-dimensional accident effect, which can provide fairly accurate accident results that represent real accident situations. Most recently, to improve the performance of trainees in a immersive environment [40], new features such as tread mills, haptic

devices, etc. are to be added in the AVR [38].

AVR-based OTSs require not only process data but also accident data to provide the trainees of CROPs and FOPs in real time. When estimating the result of accidents, computational fluid dynamics (CFD) is one of the best options since it can take into account various factors such as terrain information and fluid characteristic in three-dimensional space. A number of researchers carried out simulations of various CFD models and the performance of those models were compared with that of simpler models such as SLAB, HGSYSTEM, ALOHA. [41] [42] [43] In this viewpoint, in the next section, a new platform of the HOD process bridging process and accident simulation results with the OLE technology is introduced. The detailed structure including AVR is further discussed in Chapter 4.

3.3. Methodology

3.3.1. Interactive simulation technology

An interactive simulation model links process and accident simulation models in an entire training scenario from process upsets to accident occurrence and propagation. The architecture of the proposed interactive simulation platform is shown in Figure 3-1. In this platform, three simulations are linked based on certain sequence of accident scenarios: Dynamic process simulation, Source-term model discharge calculation, and pre-calculated 3D-CFD simulation. As the scenarios are initiated with certain process upset like equipment failure, dynamic process simulation firstly calculates the effect of the failure to the process for each time. The real-time results are automatically conveyed to the integration platform called PAISE (Process and Accident Interactive Simulation Engine). When the accident release conditions are met at certain time as an error is accumulated, source-term model built in the domain is activated to calculate the discharge at the leakage point in equipment. Calculated discharge flowrate is transmitted back to the dynamic process simulator and affects the simulator to realize the leak through generating an additional stream. As the same time, pre-calculated 3D-CFD simulation results for dispersion, fire, and explosion of discharged fluid are selectively sent to the domain for each time via the export port of a CFD database according to the leakage conditions like pressure, temperature and hole-size. This whole sequence partly by OLE technology is visualized in the training system so that trainees can see the results and take actions in it.

Through this simulation linking structure, the model leads trainees to actively analyze process variable trends based on the simulation results and take proper actions with their own decision to stabilize the variables or minimize operational losses. When stabilization fails and accident occurs, associated results like gas cloud concentration and explosion overpressure at each time and position are additionally provided to the trainees.

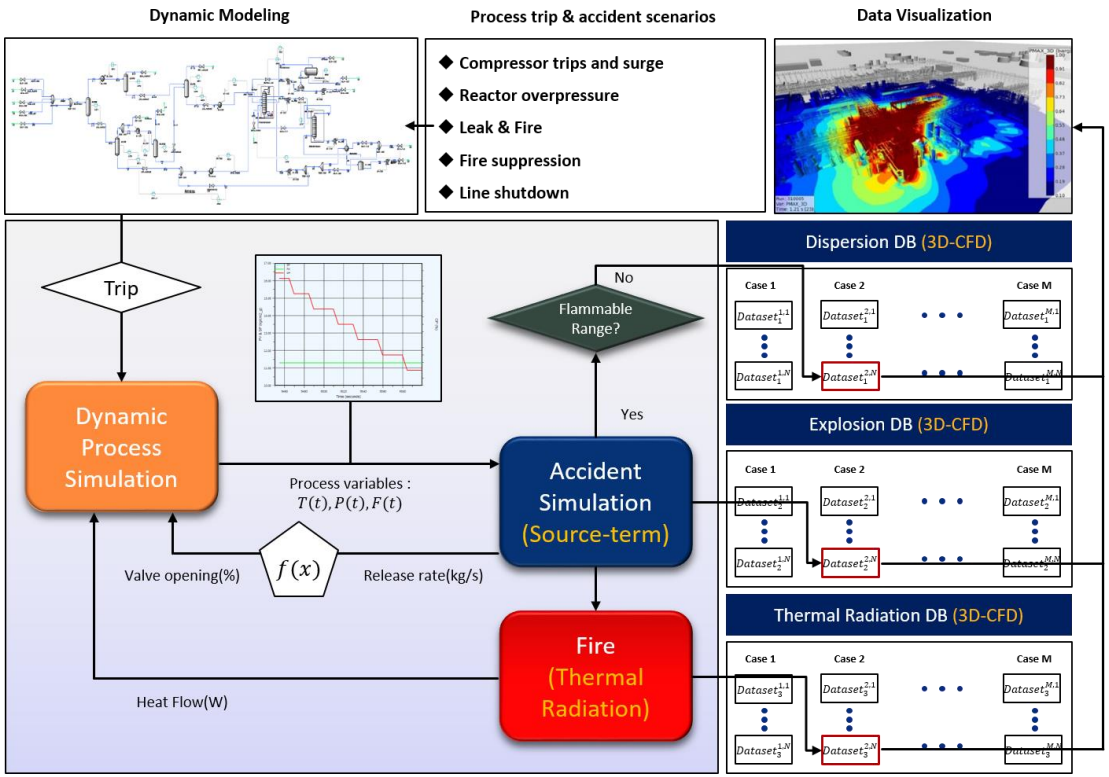

Figure 3-1. Schematic of interactive simulation technology

3.3.2. Dynamic process simulation

Dynamic process simulation using Aspen HYSYS gives trainees almost the same trend of process variables with that of a real plant. As a scenario is initiated, physical and thermodynamic calculations are conducted online and variable trends deviating from set points or being stabilized to those points can be analyzed. As errors are accumulated and the variables reach the pre-defined conditions of an accidental release scenario, values of the variables at that time are automatically inserted into the accident simulation model. When trainee' actions like emergency shutdown by clicking a manual valve in the training environment are taken, associated signal is transferred to the process simulation model so that the actions are reflected in the model.

In order to separate the linking point with process simulation model, accident simulation model is divided into two sub-models: One is 'Source-term model' calculating discharge from inside of the equipment to outside through an orifice. And the other is '3D-CFD model' calculating indoor or outdoor dispersion and fire & explosion effects after the discharge.

Source-term model calculates the release mass flowrate, F[kg/h] with given process simulation results at the time when a fluid starts to release and transfers the results to 3D-CFD model. As this release should be simultaneously reflected in the process simulation model, we generate an additional stream and a valve at the release position right behind the main valve in the process model and automatically adjust the valve openings as with Equation 3-2 and Figure 3-2 so that the fluid is to

be released with the quantity calculated from source-term model.

$$Q_1 = \ C_{disc}A\sqrt{\gamma \cdot \rho_i \cdot P_i \cdot (2/\gamma + 1)^{(\gamma+1)/(\gamma-1)}} \quad (3\text{-}1)$$

where Q_1=release mass flowrate [kg/h] in an orifice model; C_{disc}= discharge coefficient; A=hole area [m2]; γ=specific heat ratio (=C_p/C_v); ρ_i=inlet fluid density [kg/m3]; P_i=inlet pressure [kPa].

$$Q_2 = k\sqrt{V_{open} \cdot dP \cdot \rho} \quad (3\text{-}2)$$

where Q_2=mass flowrate [kg/h] from a pressure-flow relation in the valve; k=valve conductance [kg/h]; V_{open}=valve opening [%]; dP=friction delta pressure [kPa]; ρ=gas density [kg/m3].

3D-CFD model utilizes commercial software of FLACS in order to guarantee the accuracy of dispersion calculation. As CFD calculation requires heavy computational load unlike source-term model, this study develops a method of real-time processing the offline CFD data for applying the CFD model to our training system in which the real-time data transfer between the simulation model and training environment is essential. For this purpose, we construct a big database, save the CFD results in it with respect to each scenario, and provide them to trainees selectively as they take a certain action in the training interface.

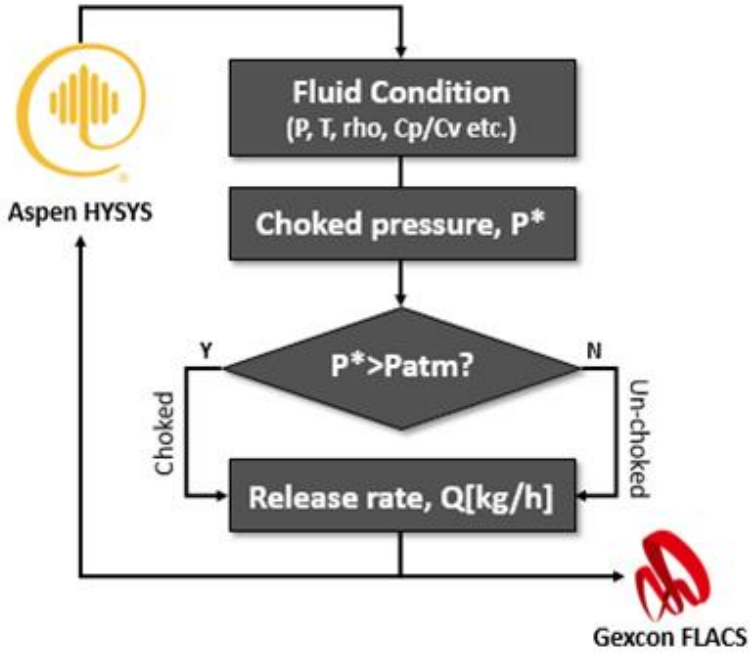

Figure 3-2. Source-term modeling

3.3.3. Accident simulation

Training with pre-defined operating scenarios and pre-calculated CFD data holds low degree of freedom in that the trainees cannot do anything but certain actions designated by the system in advance. In order to overcome this limitation, this study suggests a real-time CFD data processing method consisting of four steps described below and increases the training effectiveness of our model.

(1) Trainee Action List - Generate trainee action list in a certain scenario and process. For the case of pressure regulating station this study will address later, 'Manually close the emergency shutdown valve inside the station' is a representative action in case of a gas release.

(2) Release Duration - Determine the range of release duration based on a field operator's average site arriving time (15min for pressure regulating station) and the mission fails if the training time exceeds the maximum time (30min for the same process) without a series of proper actions.

(3) 3D-CFD Database - Divide the range of release duration (15-30min) with one minute interval, and save total 16 simulation results, labeling each gas concentration dataset $C^i(x, y, z, t)$ as $Dataset^i(i = 15, 16, \cdots, 30)$.

The structure of data processing with respect to trainee action is expressed in Equation 3-3 and Figure 3-3. As the release start ($\mathrm{t} = t_{rel}$), firstly the dataset of maximum release duration, $Dataset^{30}$ is transferred to a trainee in the training environment in real-time. The reason for the selection of this dataset is that anyone can know at which time the trainee would do the proper action. When the trainee

receives the message to move, an avatar in the program heads for the site by trainee's manipulation. When the avatar closes the shutdown valve at a certain time (t = t_{act}), the CFD data after that time are automatically replaced by those in $Dataset^{(t_{act}-t_{rel})}$ not in $Dataset^{30}$.

$$
\begin{aligned}
&C(x,y,z,t) && && (3\text{-}3)\\
&= 0 && 0 \le t < t_{rel}\\
&= C^{30}\big(x,y,z,(t-t_{rel})\big) && t_{rel} \le t < t_{act}\\
&= C^{(t_{act}-t_{rel})}\big(x,y,z,(t-t_{rel})\big) && t_{act} \le t \le t_{max}
\end{aligned}
$$

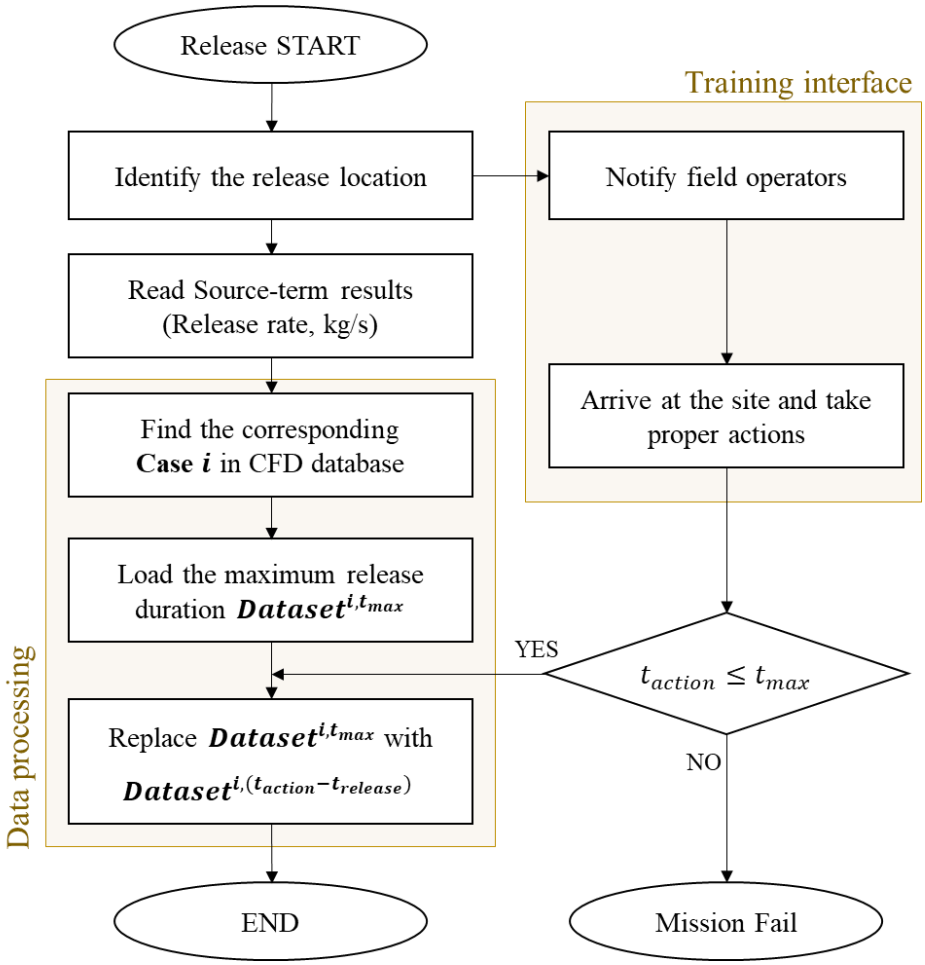

Figure 3-3. Real-time CFD data processing modeling

3.4. Construction of OTS platform: Entire HOD process

3.4.1. Target process modeling

In this Chapter, the whole HOD process including not only the reactor section, but also the separation section is modeled by Aspen HYSYS. As described in section 2.4.1, it has several subsections and there are two most representative sections: Reactor and fractionation. In the reactor section, the reactant compounds including sulfur and other impurities are hydrogenated with the aid of nickel, cobalt and other metal catalysts to be hydrogen sulfide and hydrocarbons. Make-up hydrogen is supplied to maintain the pressure of the reactor as constant and the reactor effluent is also recycled around the reactor section. The fractionation section serves as separating the reactor effluent which consists of hydrogen sulfide and other hydro carbons. It has sequential vessels to roughly separate the product first, and a distillation column at the end to rigorously separate the heavy components. The flowsheets which are constructed by Aspen HYSYS with the modified Peng-Robinson EOS are shown in Figure 3-4 and 3-5 respectively.

The parameters of the controllers are reasonably obtained by HYUNDAI Oil Bank company and other missing data are chosen with rule of thumb as in Table 3-1. Validation of the dynamic model is performed by step testing. That is, setpoints of controllers change and the trend of process variables are monitored to see if those values robustly track the changed setpoints. The step testing results are shown in Figure 3-6.

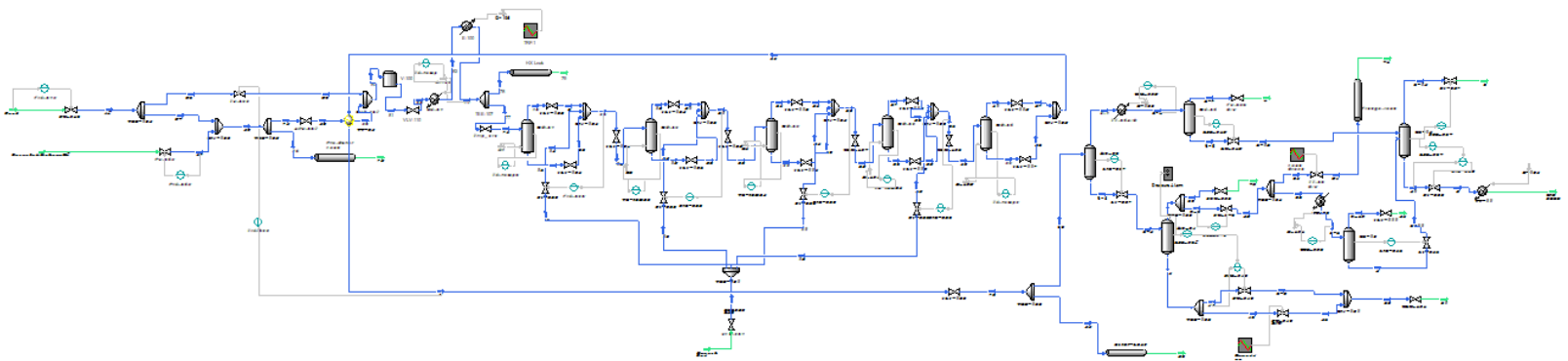

Figure 3-4. Flowsheet of reactor section

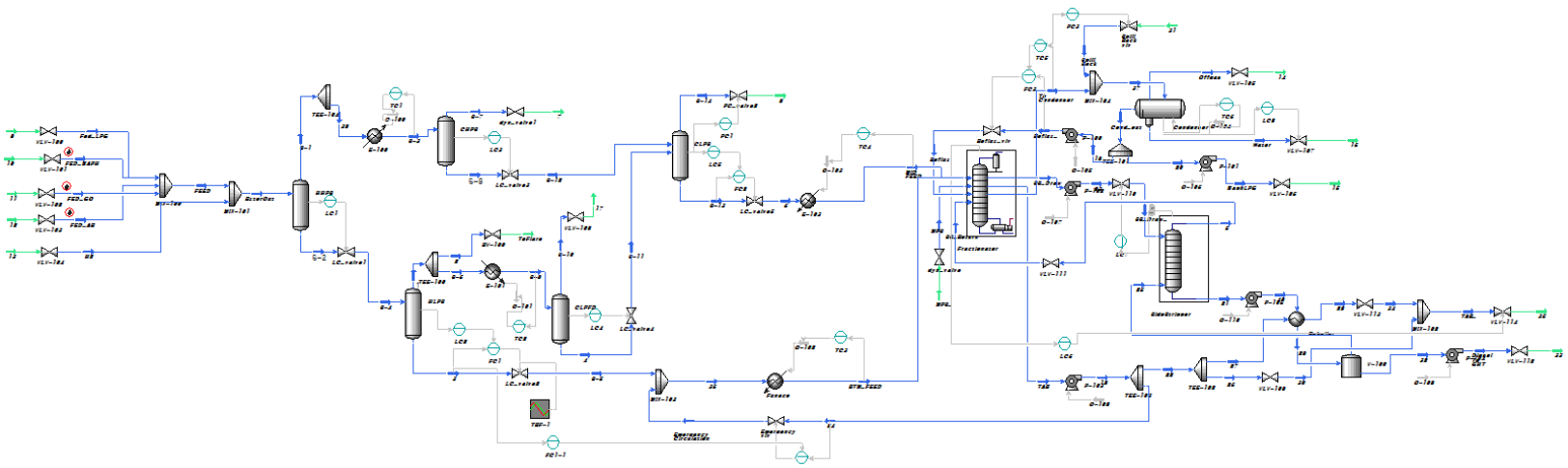

Figure 3-5. Flowsheet of fractionation section

Table 3-1. Tuning parameters of controllers

	Flow	Level	Pressure
K_c	0.5	2	2
τ_I	0.3	-	10
	Temperature		
	Liquid		Gas
Time constant	0.5		0.1
Type	First-order lag		First-order lag

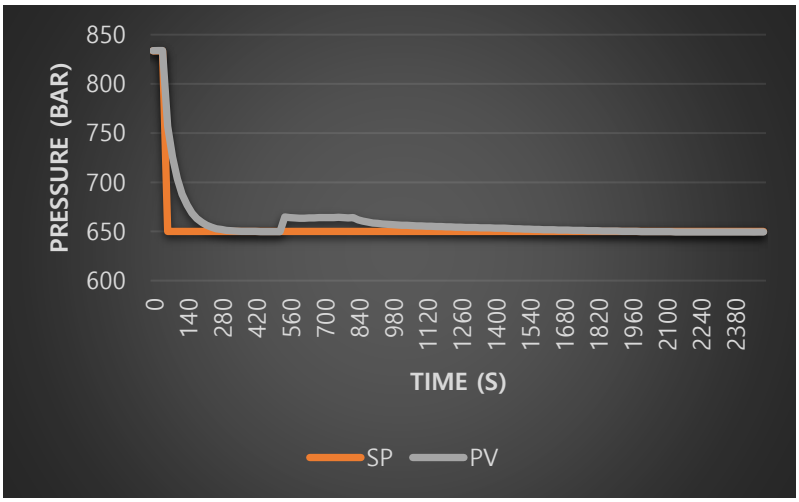

(a) Trend of SP and PV of feed pressure

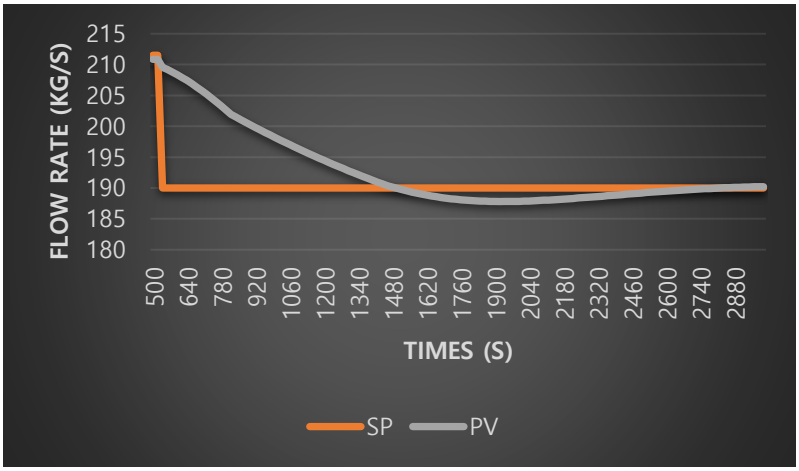

(b) Trend of SP and PV of make-up hydrogen flow rate

Figure 3-6. Setpoint tracking

3.4.2. Scenario generation: From process anomaly to accident

Scenarios are generated based on the historical data of process upsets or accidents. As these cases are documented with real process data and event sequence, scenario generation process is initiated at HAZOP and historical data of the license company. The resultant scenario tree is formulated in Figure 3-7 and 3-8 starting from top initiating event of pressure rise to the final state of process stabilization or accidents. Among all these scenarios of the HOD process, the representative scenario of release near the reactor is selected and analyzed. First, pressure rises from the make-up gas compressor. If the standby compressor operation fails to operate, hydrogen releases through pipeline flanges near the reactor. In this case, related block valves should be closed to prevent further accident propagation. If this operation also fails, fire occurs and the corresponding emergency procedure has to be conducted such make-up line isolation, bleed gas isolation, and feed line isolation. Depending on the success of failure of these sequential events, each scenario results in different branches of the scenario tree, providing various training outcomes with high degree of freedom. The representative results of process and accident simulation of the fire scenario of Figure 3-7 are shown in Figure 3-9 and Figure 3-10.

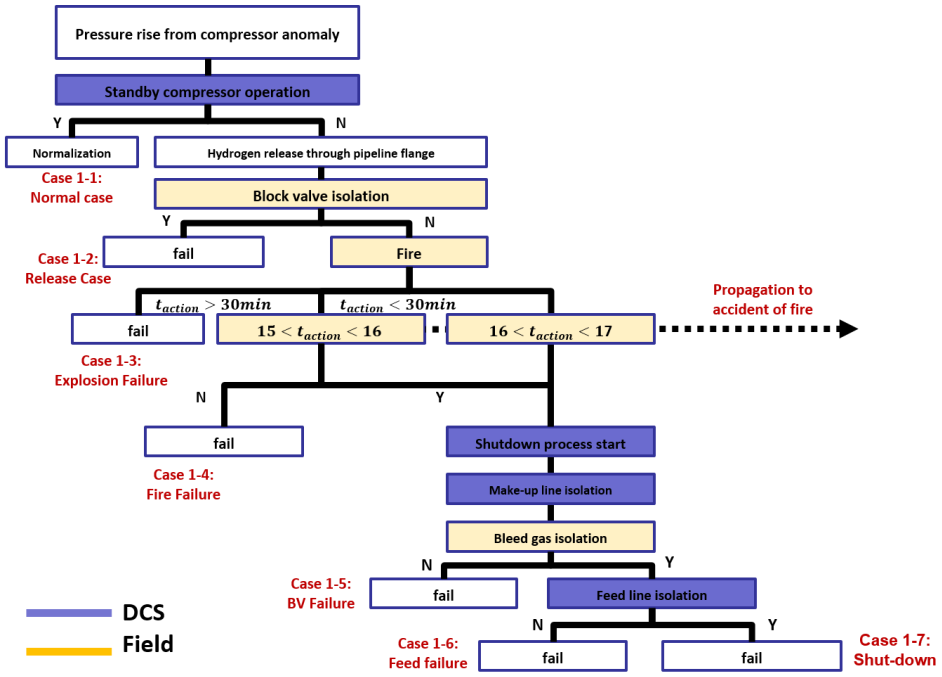

Figure 3-7. Release scenario in reactor section

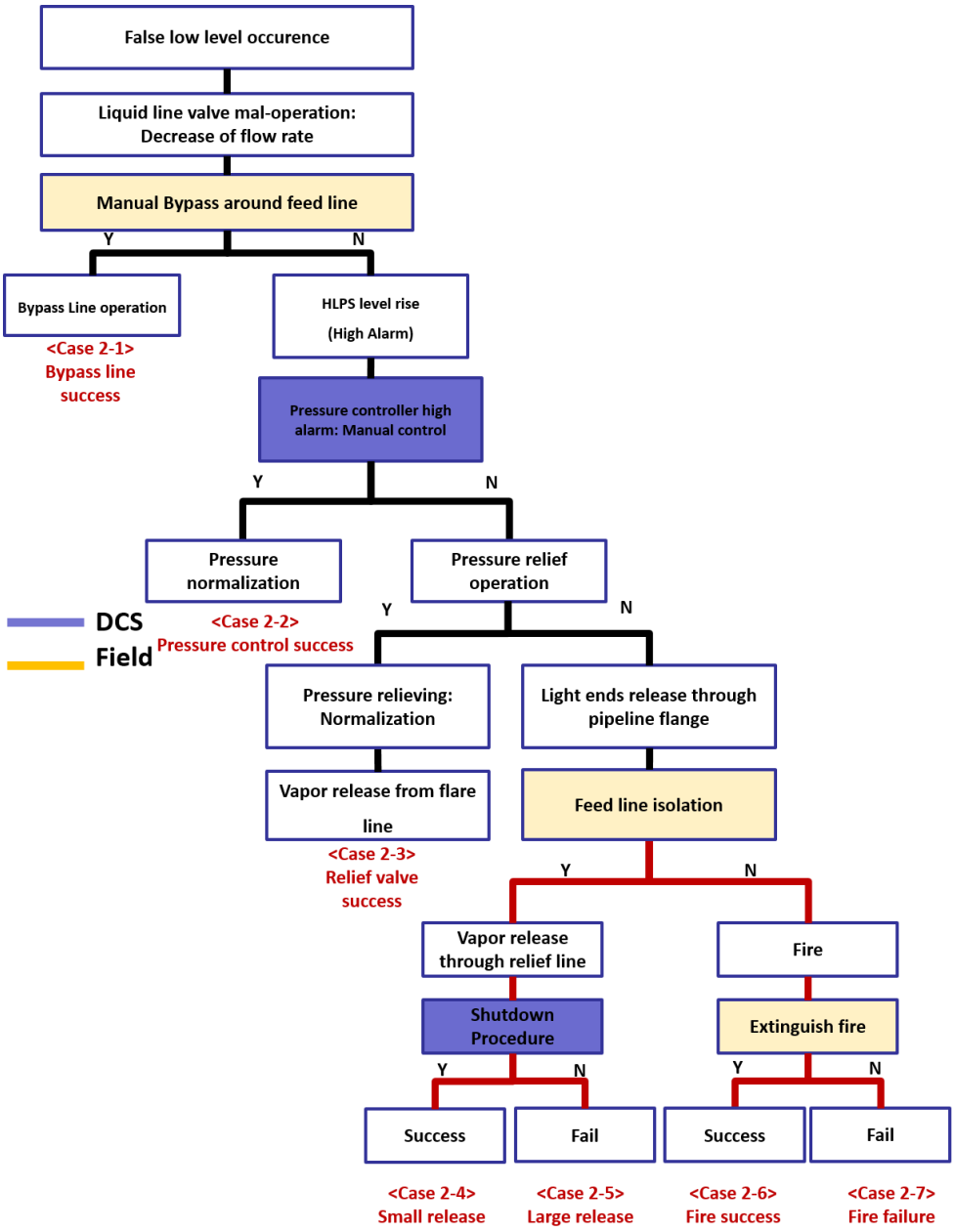

Figure 3-8. Release scenario in fractionation section

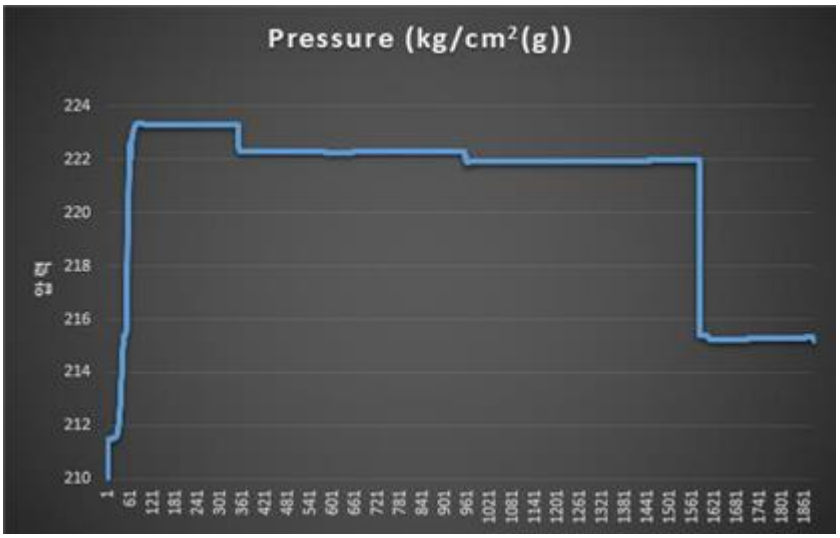

(a) Pressure trend of reactor feed stream in case of hydrogen release

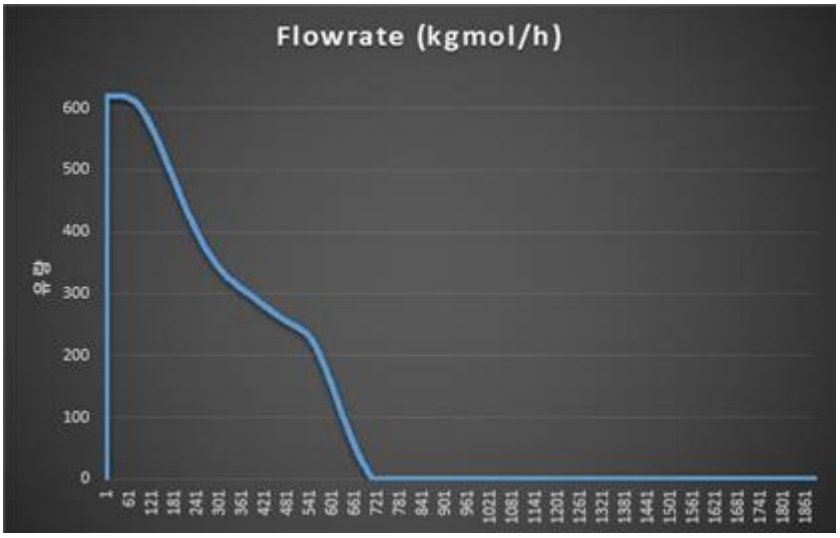

(b) Flow rate trend of reactor feed stream in case of hydrogen release

Figure 3-9. Resulting trend of process variables in case of hydrogen release

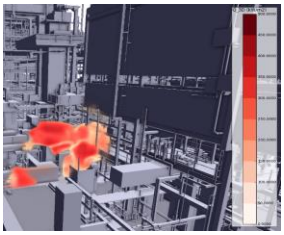

(a)-1 : 10min

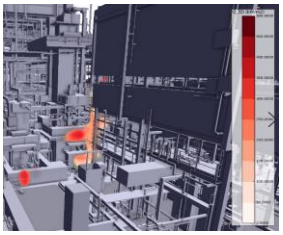

(a)-2 : 20min

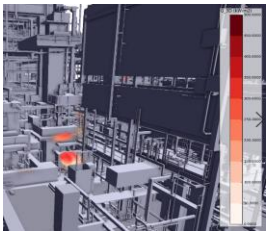

(a)-3 : 30min

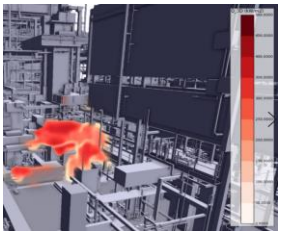

(b)-1 : 10min

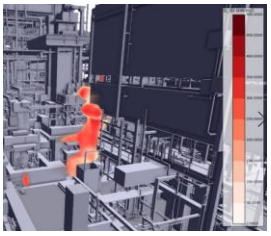

(b)-2 : 20min

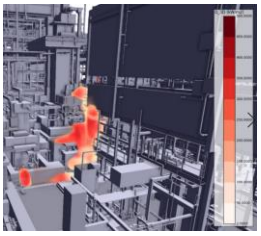

(b)-3 : 30min

Figure 3-10. Resulting trend of fire propagation: (a) $t_{action} = 15min$ **(b)** $t_{action} = 20min$

3.4.3. Interactive simulation platform

The interactive simulation platform (PAISE) is designed as in Figure 3-11. The platform was designed as most of other existing OTSs to be familiar with trainees. On the top left are three buttons which control the simulation status: The first button is to play, the second button is to pause, and the last button is to stop. In the top center is a filter in which the trainees can select training scenarios as in Figure 3-7 and 3-8. In addition, on the top right, a status panel displays the simulation state, simulation time, network state, and alarm for providing detailed information of the process during the training procedure. On the main board is the process flow diagram (PFD) of the HOD process, also, various PFDs can be shown by changing the super tabs on the top left of the main board. When a scenario start, accident information as well as process information is displayed simultaneously, to be expected an escalated training effect.

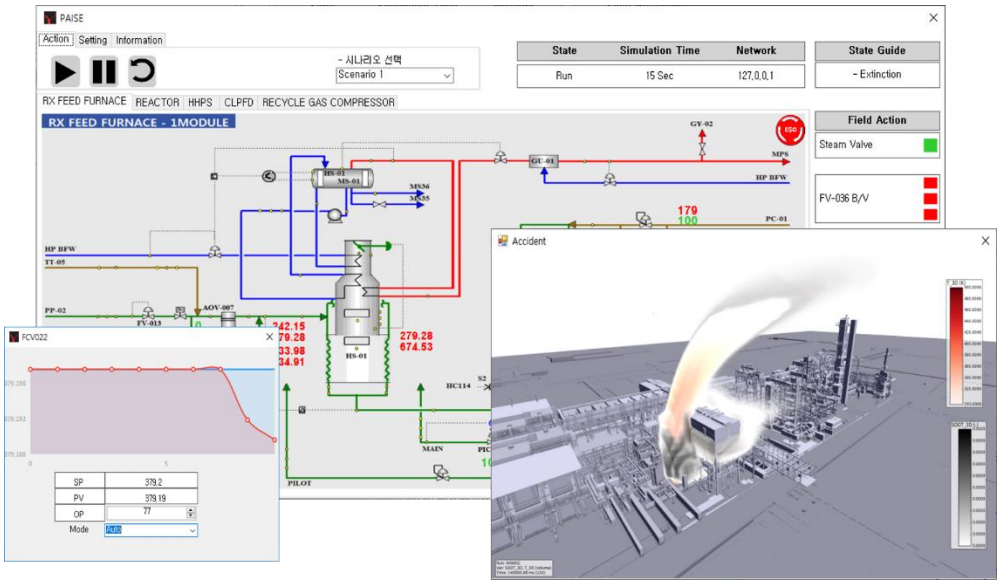

Figure 3-11. Training interface of interactive simulation platform

3.5. Conclusion

In this study, development of interactive simulation platform which will be used as an internal engine of operator training system targeting at HOD process was conducted and simple examples were shown. Developed model was designed to take correct and prompt measures depending on the process upsets and accident scenarios via OLE.

Representative scenario of ‘release scenario in reactor section and subsequent fire’ is studied as follows. When the instructor starts the scenario, pressure rises from the make-up gas compressor. If the standby compressor operation fails to operate, hydrogen releases through pipeline flanges near the reactor. In this case, related block valves should be closed to prevent further accident propagation. If this operation also fails, fire occurs and the corresponding emergency procedure has to be conducted such make-up line isolation, bleed gas isolation, and feed line isolation.

The trainee who noticed this accident is told shut-off the emergency shutdown valve manually. The actions of the trainee are displayed in the developed platform in real-time, to be providing a more efficient training performance over the conventional OTSs.

Chapter 4. Surrogate model construction for real-time application of accident results: Variational autoencoder with convolutional neural network

4.1. Introduction

The CFD-based accident models described in Chapter 3 have a fatal drawback, i.e. computation cost. Most accident scenarios need more than one hour to be calculated in tools such as FLACS and Fluent [7]. However, accident results which are provided to VR-based OTSs should be calculated very fast, since the amount of damage changes depending on the operation of trainees. For example, the size of gas cloud or fire and consequent lethality depend on how long it takes for trainees to take proper actions such as closing the block valve near the accident spot. For this reason, CFD tools have been unable to be used to provide information to AVR-based OTSs. To resolve this, surrogate or meta-models have been studied as a means of simplifying the complex structure of outcomes. Palmer et al. [44] used meta-models based on Gaussian process regression (GPR) to optimize an ammonia synthesis plant. Chen et al. [45] extended the scope of meta-models to time-space-dependent output variables in conjunction with GPR. Furthermore, Wang et al. [46] used a meta-model using GPR to CFD-simulated vapor cloud dispersion in LNG process and Loy et al. [47] introduced a linear piece-wise surrogate method and a non-linear global surrogate method for the enhancement of CFD-based consequence analysis, evaluating the performance through a case study of LNG pool fire.

4.2. Background

According to the various studies which dealt with state-of-the-art techniques for meta-modeling [48], dimensionality reduction of data is indispensable in most cases since the sheer size and complexity of the data set sometimes makes the analysis tough. The most representative method is principal component analysis (PCA) which can reduce the dimensionality of data with orthogonal basis set. However, PCA assumes that the principal components are a linear combination of the original features. Therefore, if significant non-linearity exists, PCA will not give sensible results. Autoencoders (AE) are considered as one of the possible options since it can learn non-linear transformations with non-linear activation functions and multiple layers. Moreover, it can be combined with convolutional neural network (CNN), which results in the significant improvement on performance [49] [50]. Most recently, a new methodology of variational autoencoders (VAE) which utilize the latent space concept generated by the features of training data emerged as a powerful tool in dimensionality reduction area. [51] With a stochastic distribution which are obtained from the deterministic vectors of the internal representation, it shows an immense performance in feature extraction.

After carrying out dimensionality reduction, a regression process should be performed which evaluates each of parameters in the layers. Recently, deep neural networks (DNN) which have multiple hidden layers have improved in performance with the resolution of vanishing and exploding gradient, overfitting, and low learning rates [52]. Gloro et al. [53] proposed a way to significantly alleviate the

vanishing and exploding gradients problems by Xavier and He initialization and various activation functions such as ReLU, leaky ReLU, ELU, etc. were suggested as substitute for the conventional sigmoid activation function. Moreover, Ioffe et al. [54] proposed a technique called batch normalization (BN) to further address the vanishing and exploding gradients problems. Finally, a number of optimization algorithms such as momentum optimization, Nesterov Accelerated Gradient, AdaGrad, RMSProp, and Adam Optimization have been developed to optimize the parameters of DNNs. In particular, Adam which, stands for adaptive momentum estimation, combines the ideas of momentum optimization and RMSProp outstands other algorithms. [55]

In this study, an AVR-based OTS is developed for the heavy oil desulfurization (HOD) process in Seosan city, South Korea. To provide process and accident information with the aim of educating both CROPs and FOPs, process simulation and accident simulation are performed with commercial software of Aspen HYSYS and FLCAS respectively. In particular, a surrogate model of accident results of jet fire is proposed with data generated by FLACS to supply the accident information to trainees in real time, namely, provision of real-time damages that an avatar in the virtual space undergoes. To construct the proposed surrogate model, scenarios with four inputs of wind speed, wind direction, release duration, and time step are simulated with FLACS and the results of total heat flow flux are expressed in two-dimensional image forms. These data are then compressed using a VAE with deep convolutional layers and undergoes a regression process with a DNN. As a result, a surrogate model is constructed and the performance is compared with that of other

commonly used models. Afterwards, this resulting model which can compute outputs from any inputs very fast, serves as a tool to bridge accident results with virtual realities in real time. With this framework, an integrated AVR-based OTS is accomplished which features complex process dynamics and accident results.

4.3. AVR-based OTS platform and jet fire CFD model

4.3.1. Architecture of the proposed OTS with AVR

As described in the previous section, the AVR-based OTS to be developed aims to educate both CROPs and FOPs, therefore, the coupling of process and accident simulations is essential to provide comprehensive information to two types of trainees, i.e. CROPs and FOPs. The architecture of the proposed AVR-based OTS is shown in Figure 4-1. There are two main platforms in the architecture: Distributed control system (DCS) platform and AVR platform. The DCS platform aims to train CROPs, therefore, changes of process variables can be monitored in the DCS platform while the AVR platform serves as training FOPs in immersive training environment. The DCS platform also serves as a bridge to connect each of dynamic process model, accident model, and AVR platform. In the DCS platform, training scenarios which include process trips and resulting accidents are defined. In this paper, an abnormal process situation with pressure rise which results in release and subsequent jet fire is adopted as the training scenario. When the training procedure starts, the process variables such as temperature, pressure, and flow rate are calculated dynamically according to the pre-determined scenario by Aspen HYSYS. These values are transferred to the DCS platform to provide process information to CROPs and also used for calculating the input of the accident model by Equation 3-1.

With the calculated release rate, a CFD-based jet fire accident is modeled by FLACS and the resulting heat flux (Q) data are produced. However, as described

earlier, CFD-based models require so high computation cost that this kind of models cannot be used directly in the systems in which data should be generated very fast, almost in real time. Therefore, a surrogate model which can replace the CFD-based jet fire model is constructed, the details of which are introduced in the later sections. Then the heat flux data obtained from the surrogate model are transferred to the AVR platform, in which, a trainee with immersive gears such as haptic, navigation, optical, and acoustic devices walks around the virtual environment. In this situation, both CROPs and FOPs are instructed to take proper actions with process and accident information. For example, when a trainee approaches the accident site to follow the instruction, s/he obtains process information through various components installed in the virtual environment (e.g. changes of pressure gauge value) in addition to lethality information which is calculated by the accident result of heat flux from the DCS platform. Moreover, if the trainee take any actions such as closing valves in the AVR platform, the opening percent changes of valves are also transferred to the DCS platform and cause subsequent changes over the whole architecture. Through this process which bridges among process simulation, accident simulation, and virtual environment in real time, an improved training effect which can cover both CROPs and FOPs with communication of each other is expected [56].

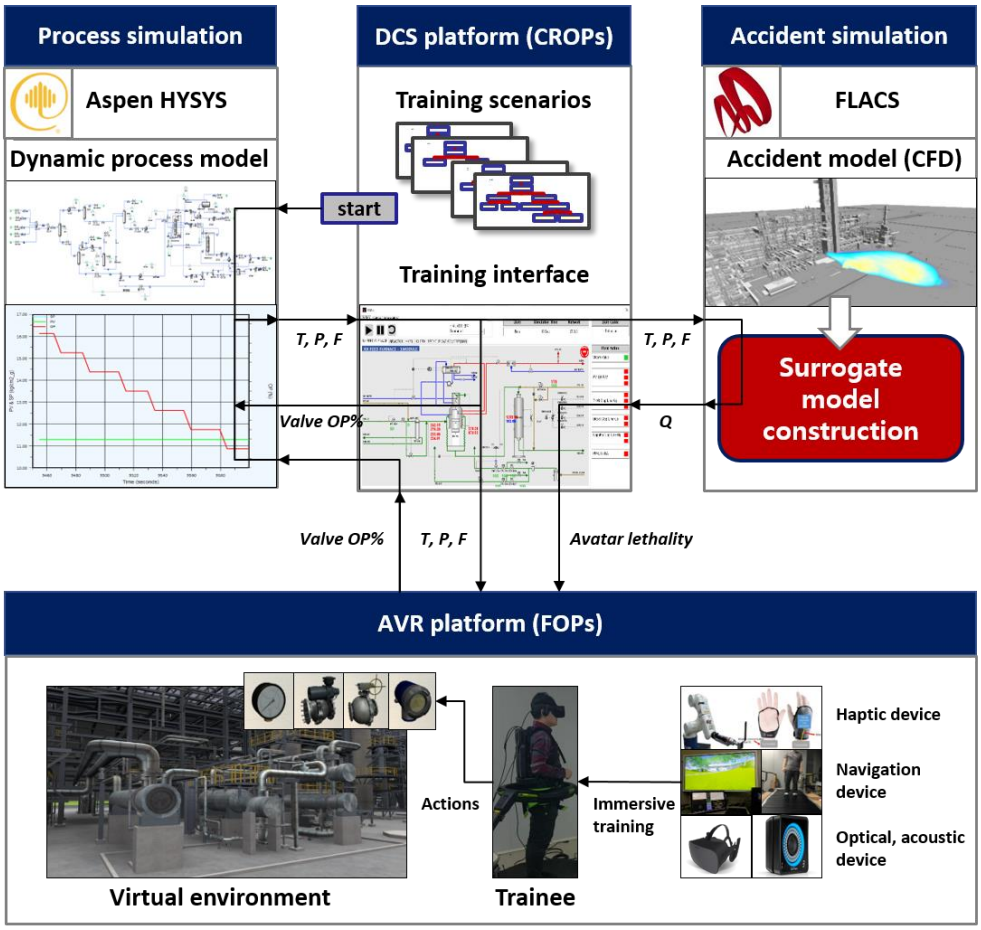

Figure 4-1. Architecture of the proposed AVR-based OTS

4.3.2. Target accident model description

The most frequent accident in the process according to the hazard and operability (HAZOP) report from the license company is a release of hydrogen and light hydrocarbon gases through pipeline flanges near the reactor which is operated in extreme conditions as mentioned above, and subsequent jet fire. Therefore, this sequence of accidents is adopted as the training scenario. Prior to constructing a surrogate model for real-time updating of accident information, sufficient data should be obtained with FLACS. The original use of FLACS was for explosion simulation on offshore oil platform. However, it increasingly expanded the simulation scope to dispersion and fire simulation. Various studies have been carried out to validate the accuracy of simulation results of FLACS. Middha et al. [57] conducted validation of hydrogen dispersion in a range of different conditions. Hansen et al. [58] presented the validation work of FLACS from source model to dispersion model in LNG spill conditions. In addition, Skarsbø et al. [59] implemented an experimental study of pool fires and validation of fire models.

The size of the entire simulation domain is 50m, 50m and 30m in the x, y, and z-direction respectively with a uniform grid of 1.6 m×1.6 m×1.6 m. The location of the release point can be identified in Figure 4-2. Simulation inputs which are chosen to create distinct outputs are wind direction from 0 to 2π, wind speed from 0.5 to 5 m/s and release duration from 60 to 180 s. Other variables are fixed through the entire simulation. The detailed simulation conditions are listed in Table 4-1.

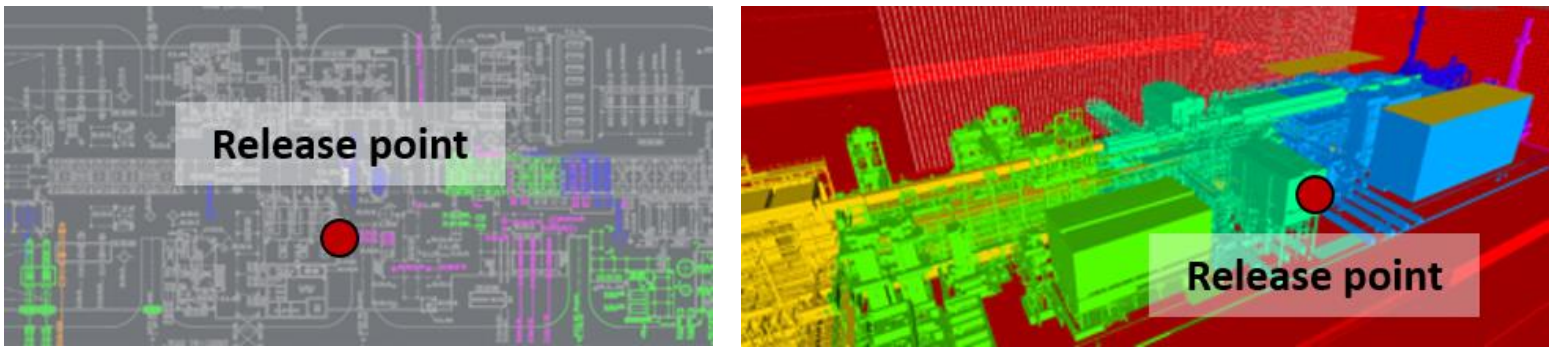

(a) Plot plan **(b) 3D view of CAD image in FLACS**

Figure 4-2. Geometry of HOD process

Table 4-1. Scenario conditions

Variable	Value
Ambient temperature	25 ℃
Ambient pressure	1 bar
Wind direction	0-2π
Wind speed	0.5-5 m/s
Discharge rate	14.4 kg/s
Release duration	60-180 s
Pasquill class	None
Total simulation time	180 s

4.3.3. Mathematical formulation of jet fire

FLACS interprets the compressible fluid flow in the solid geometry using conservation of mass and momentum.

$$\frac{\partial}{\partial t}(\beta_v \rho) + \frac{\partial}{\partial x_j}(\beta_j \rho u_j) = \frac{\dot{m}}{V} \tag{4-1}$$

$$\frac{\partial}{\partial t}(\beta_v \rho u_i) + \frac{\partial}{\partial x_j}(\beta_j \rho u_i u_j) = -\beta_v \frac{\partial P}{\partial x_i} + \frac{\partial}{\partial x_j}(\beta_j \sigma_{ij}) + F_{o,i} + \beta_v F_{w,i} + \beta_v(\rho - \rho_0) g_i \tag{4-2}$$

$$F_{o,i} = -\rho \left|\frac{\partial \beta}{\partial x_i}\right| u_i |u_i| \tag{4-3}$$

$$\sigma_{ij} = \mu_{eff}\left(\frac{\partial u_i}{\partial x_j} + \frac{\partial u_j}{\partial x_i}\right) - \frac{2}{3}\delta_{ij}\left(\rho k + \mu_{eff}\frac{\partial u_k}{\partial x_k}\right) \tag{4-4}$$

$$\mu_{eff} = \mu + \rho C_\mu \frac{k^2}{\varepsilon} \tag{4-5}$$

Turbulence is modeled by the *k*-*ε* model. It is an eddy viscosity model that solves two additional transport equations; one for turbulent kinetic energy and one for dissipation of turbulent kinetic energy. Following Boussinesq eddy viscosity assumption, an eddy viscosity models the Reynolds stress tensor as follows:

$$-\rho\widetilde{u_i'' u_j''} = \mu_{eff}\left(\frac{\partial u_i}{\partial x_j} + \frac{\partial u_j}{\partial x_i}\right) - \rho\frac{2}{3}k\delta_{ij} \tag{4-6}$$

FLACS estimates the behavior of fire with several methods. For most fires, the combustion rate is controlled by the mixing of fuel and air, and simple Mixed Is Burnt (MIB) combustion models can be applied. The transport equation for the fuel mass fraction is written as follows:

$$\frac{\partial \bar{\rho}\tilde{Y}_{fuel}}{\partial t} + \frac{\partial \bar{\rho}\tilde{Y}_{fuel}\widetilde{u_j}}{\partial x_j} = \frac{\partial}{\partial x_j}\left(\bar{\rho}D\frac{\tilde{Y}_{fuel}}{\partial x_j}\right) - \frac{\partial}{\partial x_j}\left(\bar{\rho}\widetilde{Y_{fuel}'' u_j''}\right) + \rho\widetilde{w}_{fuel} \tag{4-7}$$

The current model for the turbulence-chemistry interaction is the Eddy Dissipation Concept (EDC) [60]. It models the interaction between turbulent flow and chemical reactions.

4.3.4. Numerical setup and data preparation

FLACS uses the finite volume method to solve the conservation equations for each cell of the three-dimensional Cartesian grid. The numerical time step algorithm that is used in FLACS is based on the implicit first-order backward Euler method. Time steps in transient simulations should be set in order that the solution evolve smoothly and stably in time. The Courant-Friedrich-Levy (CFL) number provides a solver-specific criterion for the maximum time step that yields a stable solution in the compressible solver of FLACS. Two CFL numbers are used to determine the maximum time steps: CFLV and CFLC. CFLV is based on fluid velocity, whereas CFLC is based on sound velocity. The CFD solver chooses the minimum value between CFLV and CFLC. In this study, CFLV is fixed at 2 and CFLC is fixed at 20, which are common values in fire simulations.

$$\Delta t_v = \frac{\mathrm{CFLV}}{\max(\frac{u_i}{\Delta x_i})} \tag{4-8}$$

$$\Delta t_c = \frac{\mathrm{CFLC}}{\max(\frac{c}{\Delta x_i})} \tag{4-9}$$

$$\Delta t = \min(\Delta t_v, \Delta t_c), \tag{4-10}$$

To obtain hundreds of data points required for training, a procedure of sampling input variables, extracting result, and post-processing is proposed as in Figure 4-3. First, three input variables of wind speed, wind direction and release duration of which the ranges are listed in Table 4-1 are randomly sampled by Latin hypercube method [61]. With these variables, FLACS input files of CS and CL which are generated and simulations are performed 785 times which is the number of samples.

After the simulations are complete, the resulting r3 files are transformed to a3 files for easier use of post-processing. From the a3 files, Q values $(28 \times 28 \times 180)$ of which the dimension corresponds to x and y coordinates and the number of time steps respectively are extracted. Since the height that affects directly to a person is near 2 m, the values of z coordinate are not used except at the point z = 1.6 m. Finally, the data are shifted and rescaled so that they end up ranging from 0 to 1 as the following equation:

$$Q_{scaled} = \frac{Q - Q_{min}}{Q_{max} - Q_{min}} \tag{4-11}$$

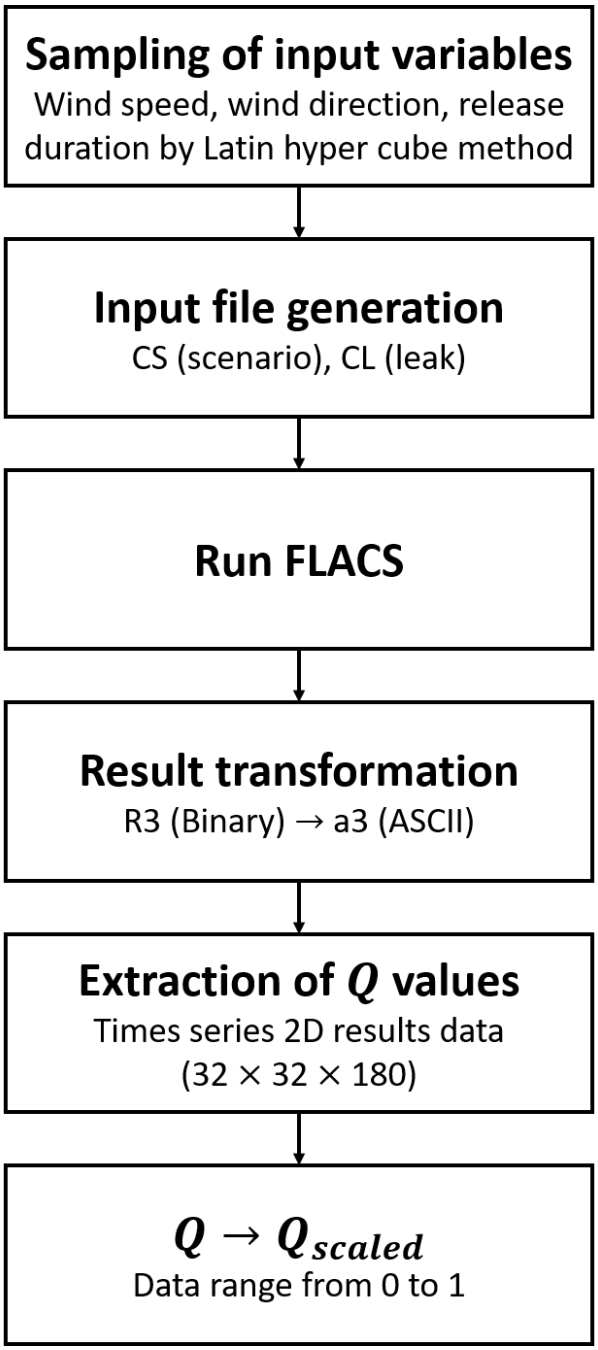

Figure 4-3. Flow chart of data processing

4.4. Surrogate model construction by VAEDC-DNN model

To build a surrogate model that can replace the jet fire CFD model, input and output have to be defined first. As described in section 2.4, the input of the original CFD model is wind speed (m/s), wind direction (rad), and release duration (s). However, one more input of time step (s) is added to the input of the proposed surrogate model to consider time series outcomes, leading to the four-dimensional input space which is represented as $v \in \mathbb{R}^{1\times4}$. The output of the surrogate model is the same as the original CFD model, which is two-dimensional contour images of Q_{scaled} represented as $x \in \mathbb{R}^{28\times28}$. Thus, the goal of the surrogate model is to map the input space v to the output space x using the pre-calculated datasets from the jet fire CFD model. To achieve the high performance model, it consists of two parts: VAEDC and DNN, where the former part serves as compressing and reconstructing the data and the latter part serves as generating a regression model with compressed data. Among the total 785 data points, 560 samples are used as training set $(v^{\text{train}}, x^{\text{train}})$ and 140 samples are used as validation set $(v^{\text{validation}}, x^{\text{validation}})$. To evaluate the performance of the trained model, 85 samples are used as test set $(v^{\text{test}}, x^{\text{test}})$.

4.4.1. VAEDC-DNN model description

PCA has been one of the most widely used methods to reduce data of high dimensions and extract features in various fields of chemical engineering. [62] [63] [64] [65] [66] However, since it turned out that deep autoencoder networks learn low-dimensional codes that work better than PCA [67], well-trained deep autoencoders have been introduced in the recent studies [68] [69]. Unlike PCA, autoencoders can learn non-linear transformations with non-linear activation function and multiple layers. In fact, training an autoencoder with one dense encoder layer, one dense decoder layer, and linear activation function is essentially equivalent to performing PCA. Moreover, due to the relationship with the latent variable model [70], autoencoders can be considered as generative models which can extract complex features of not only deterministic data but also stochastic data. Given the advantages of autoencoders, a variational autoencoder which consists of a probabilistic encoder ($q_\phi(z|x)$) and a probabilistic decoder of the generative model ($p_\theta(x|z)$) derived from variational Bayes is introduced [51]. As a result, a variational autoencoder with deep convolutional layer (VAEDC) is proposed, of which the architecture is shown in Figure 4-4.

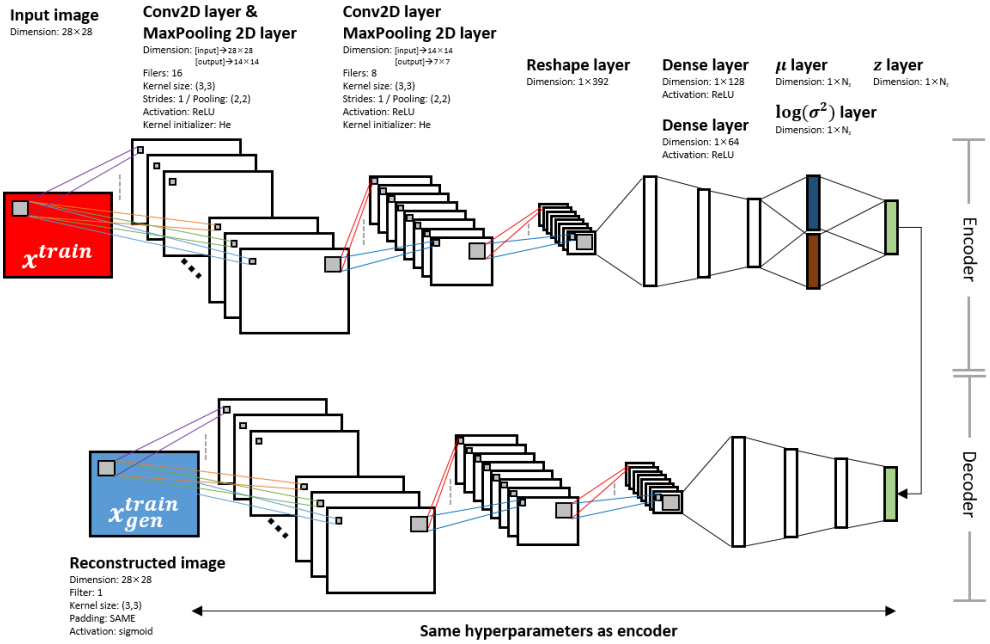

Figure 4-4. VAEDC architecture

Two convolutional layers with a kernel size of (3, 3), stride of 1, He initialization, and ReLU activation function are constructed to extract features from the input image with the aid of 16 and 8 filters in the first and second convolutional layer respectively. After each layer, a max pooling with (2, 2) filters and stride of 2 is applied, leading to the reduction of the input image dimension from (28×28) to (7×7). The resulting $(7 \times 7 \times 8)$ image is reshaped into (1×392) to build a series of 392-128-64 dense layer with ReLU activation function. Subsequently, two parallel layers of μ and $\log(\sigma^2)$ are constructed, each represents mean and log of variance of the latent variables respectively. N_z represents the number of latent variables and accordingly, the dimension of the μ and $\log(\sigma^2)$ layers is $1 \times N_z$. From these two layers, the mean and log of variance of latent variables are sampled and combined in the z layer as a vector to fit the decoder network. However, since backpropagation cannot be conducted through a sampling node, a reparameterization trick was proposed in the previous study [51], and the actual z vector is calculated as the following equation:

$$\mathrm{z}^{(i)} = \mu^{(i)} + \sigma^{(i)} \odot \epsilon, \ where \ \ \epsilon \sim \mathcal{N}(0,1) \tag{4-12}$$

Where ϵ signifies a Gaussian distribution with mean of 0 and standard deviation of 1. Following this encoding process, the decoding process is performed which is the exact inverse of the encoding process.

When reconstruction work through the decoder is finished, the loss between x^{train} and x_{gen}^{train} should be calculated to further train the model parameters. In this study, the loss function of variational lower bound on the marginal likelihood is

used as proposed in the previous study. [51]

$$\mathcal{L}(\theta, \phi; \mathrm{x}^{(i)}) = -D_{KL}(q_\phi(z|x^{(i)})||p_\theta(z)) + \mathbb{E}_{q_\phi(z|x)}[\log p_\theta(x^{(i)}|z)] \quad (4\text{-}13)$$

Where $-D_{KL}$ represents Kullback-Leibler (KL) divergence, $p_\theta(x|z)$ is the probabilistic decoder with the generative parameter θ, and $q_\phi(z|x)$ is the probabilistic encoder with the variational parameter ϕ. In addition, it has been proved that the KL divergence can be computed and differentiated without estimation. With the combination of Equation 13, the loss function finally can be approximated as below:

$$-\mathcal{L}(\theta, \phi; \mathrm{x}^{(i)}) \simeq -\frac{1}{2}\sum_{j=1}^{N_z}(1 + \log\left(\left(\sigma_j^{(i)}\right)^2\right) - \left(\mu_j^{(i)}\right)^2 - \left(\sigma_j^{(i)}\right)^2)$$
$$+ \frac{1}{N_{\text{train}}}\sum_{l=1}^{N_{\text{train}}} \log\ p_\theta(x^{(i)}|z^{(i,l)}\ ) \quad (4\text{-}14)$$

Where the minus term on the left side is added to convert the maximization loss problem of Equation 14 to a minimization problem.

The DNN serves as generating a regression model which maps the variable space (wind speed, wind direction, release duration, and time step) to the latent space, of which the architecture is shown in Figure 4-5. The total number of 4 fully connected hidden layers is used with batch normalization, ReLU activation function, and He initialization. The data points used in training and validating the DNN are randomly resampled denoted as $(v^{train'}, x^{train'})$ and $(v^{validation'}, x^{validation'})$. The number of training sets is 560 and the number of validation sets is 140, which is the same as the originally sampled $(v^{\text{train}}, x^{\text{train}})$ and $(v^{\text{validation}}, x^{validation})$. The loss function of the DNN model is a simple mean squared error equation as follows:

$$MSE = \frac{1}{N_{train}} \sum_{i=1}^{N_{train}} (z - z_{gen})^2 \quad (4\text{-}15)$$

Where z is obtained from $x^{\text{train}'}$ using the pre-trained VAEDC model

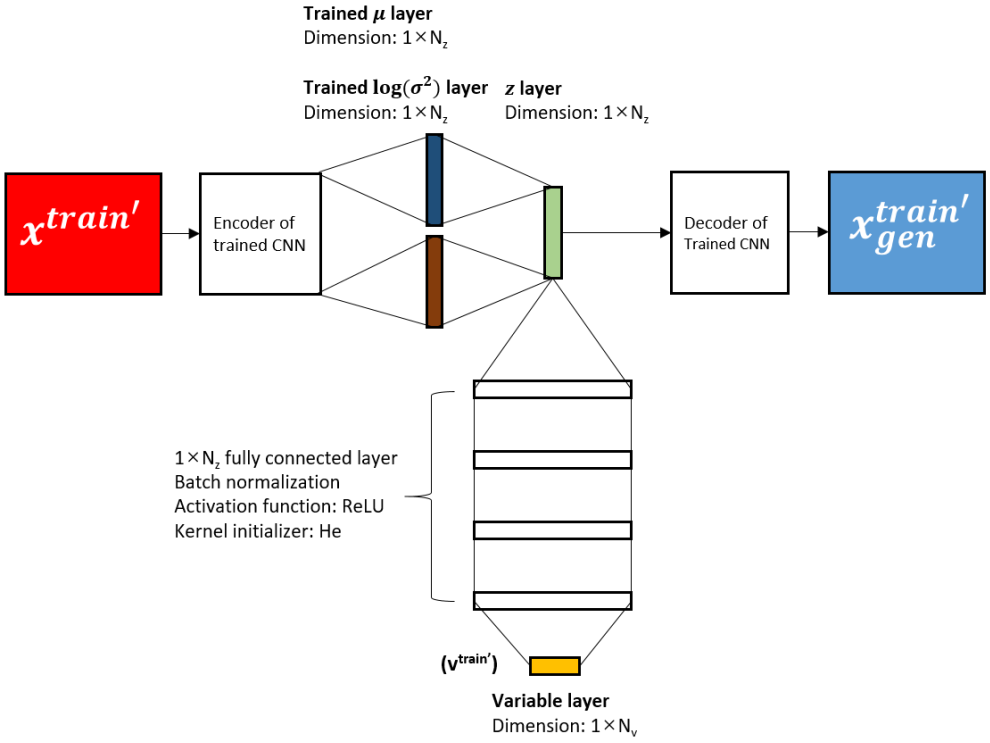

Figure 4-5. DNN architecture

4.4.2. Numerical setting

To evaluate the performance of the entire VAEDC-DNN model, the test data sets sampled from section 4.4.1. are used. The mean squared error equation is adopted to assess whether not only the latent space effectively represents the original space, but also the mapping of the variable space to the latent space is accurately performed.

$$MSE = \frac{1}{N_{test}} \sum_{i=1}^{N_{test}} (z - z_{gen})^2 \quad (4\text{-}16)$$

Moreover, the performance of resulting model is compared with that of other simpler models which are based on autoencoders and neural networks: a neural network with one hidden layer (NN) without autoencoder, a deep neural network with three hidden layers and batch normalization (DNN) without autoencoder, NN with simple autoencoder (AE-NN), NN and DNN with deep convolutional autoencoder (DCAE-NN, DCAE-DNN), DNN with simple variational autoencoder (VAE-DNN), and DNN with variational autoencoder with deep convolutional layers (VAEDC-DNN). The detailed information of each model is listed in Table 4-2.

Table 4-2. Various surrogate models for comparison of VAEDC-DNN model performance

	NN	DNN	AE-NN	DAE-NN	DAE-DNN	AEDC-NN	AEDC-DNN	VAE-DNN	VAEDC-DNN
Dimensionality reduction part description	-		One fully connected dense layer	5 fully connected hidden layers		5 fully connected hidden layers, 2 convolutional layers with max pooling		5 dense layers with one variational layer	7 fully connected hidden layers, 2 convolutional layers with max pooling
Loss function	-		Binary cross entropy					Variational lower bound	
Regression part description	One fully connected hidden layer	Three fully connected hidden layers with BN	NN	NN	DNN	NN	DNN	DNN	DNN
Loss function	Mean squared error								

4.5. Results and discussion

4.5.1. Performance evaluation

In Table 4-3, the mean squared error values between x_{gen}^{test} and x^{test} for each of the 75 newly sampled test data sets (x^{test}, v^{test}) are listed. The VAED-DNN model showed the highest performance, which signifies that it not only memorizes the overall shape of the images, but also extract complex features with efficient mapping from the variable space to the latent space. It can be also identified in Table 4-3 that the performance is improved even when NN is used in the order of VAE, DCAE, DAE, and AE. This phenomena show the great power of VAE-based surrogate models with combination of CNN. The NN and DNN which are devoid of VAE: dimensional reduction part, extremely showed poor performance over the other models. To visualize the performance, the reconstructed images by various surrogate model is shown in Figure 4-6.

Table 4-3. Mean squared error of various surrogate models

Dimensionality reduction part	-		AE	DAE		AEDC		VAE	VAEDC
Regression part	NN	DNN	NN	NN	DNN	NN	DNN	DNN	DNN
Batch normalization	w/o	w/	w/o	w/o	w/	w/o	w/	w/	w/
MSE	0.00884	0.00424	0.0125	0.00851	0.00341	0.007125	0.00251	0.00253	0.00235

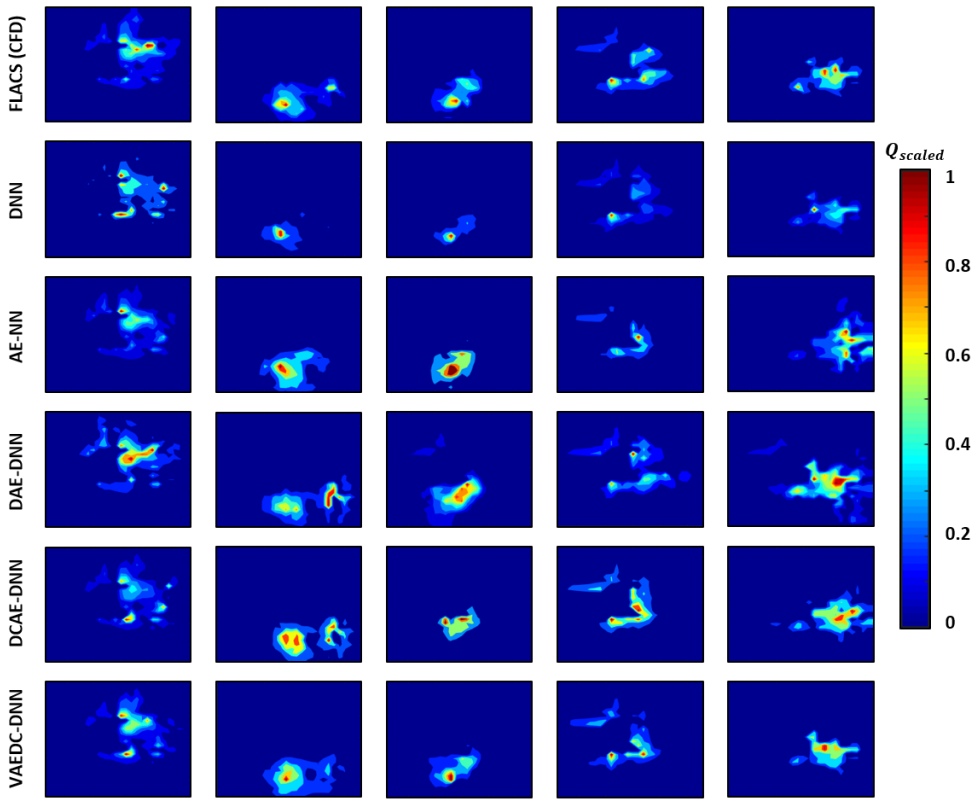

Figure 4-6. 2D contour of various surrogate models

In each column, randomly selected x_{gen}^{test} 2D contour images for DNN, AE-NN, DAE-DNN, AEDC-DNN, and VAEDC-DNN constructed from FLACS (CFD) is shown. When NN or DNN without dimensionality reduction is used, the resulting surrogate models show poor performance, which means those regression-only models cannot extract the feature of the original images efficiently. Moreover, due to the characteristics of non-linear complexity of the images, it is even difficult to reconstruct the overall, macroscopic shape of the images with the regression-only models. This can be especially seen in the second and fourth columns in Figure 4.6. In the surrogate models with dimensionality reduction part: AE and VAE, enormous performance improvement can be identified. However, some models still show trouble in predicting images. The AE-NN model belongs to this case. The approximate trends are quite correct, however, in the case of fifth column, prediction is considerably inaccurate. Looking at the overall trend from Table 4-3 and Figure 4-6, introduction of batch normalization serves as a huge means for advancing the surrogate model performance. Furthermore, the importance of convolutional layers can be also seen for efficient extraction of complex features. The two best models, i.e., DCAE-DNN and VAEDC-DNN, provide superior predictions over the other models. Between these models, VAEDC-DNN model shows better performance and it can be seen in the first column, in which Q_{scaled} spreads out with fine boundaries. The VAEDC-DNN model is able to detect feature which are undetectable in the AEDC-DNN model. In conclusion, superior feature extraction is achieved even when the images have complex patterns.

4.5.2. Application to AVR-based OTS

Figure 4-7 briefly describes the configuration of the VAEDC-DNN surrogate model and shows how it works when inserted in the AVR-based OTS. When the training start, jet fire occurs with randomly selected input variables: Wind speed and wind direction. In this manner, for each training situation, the operator is under different situations with various circumstances. With the selected inputs, Q is calculated with the VAEDC-DNN surrogate model at a significant rate, almost real time. From the obtained Q values, avatar lethality is calculated and the information provided to the AVR, through the OLE technology which was introduced in Chapter 3. When the trainee takes action, changes to the accident results occur and this outcome is also reflected to the AVR. The input of time steps in this study is just 180s, however, it can be expanded to large time steps and generate more sophisticated results. The visualization of jet fire results with combination of other wearable devices in AVR is shown in Figure 4-8, which can provide an efficient and improved training effect over the conventional OTSs.

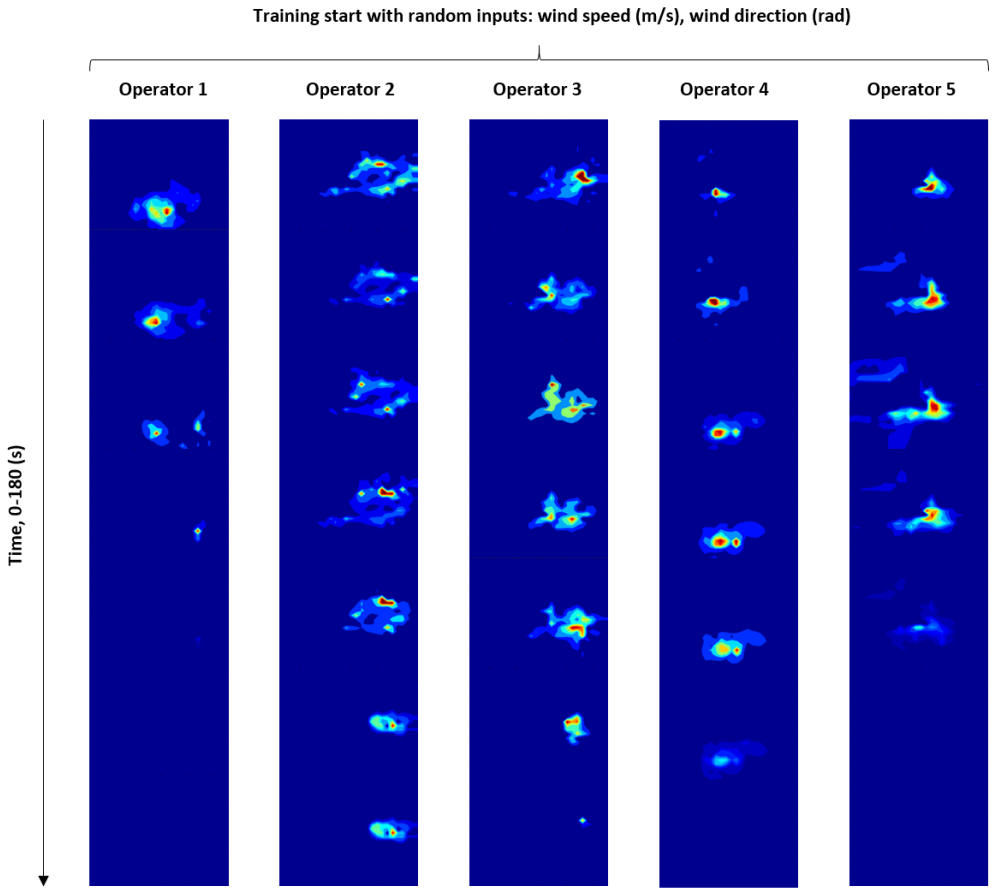

Figure 4-7. Training scheme with VAEDC-DNN surrogate model

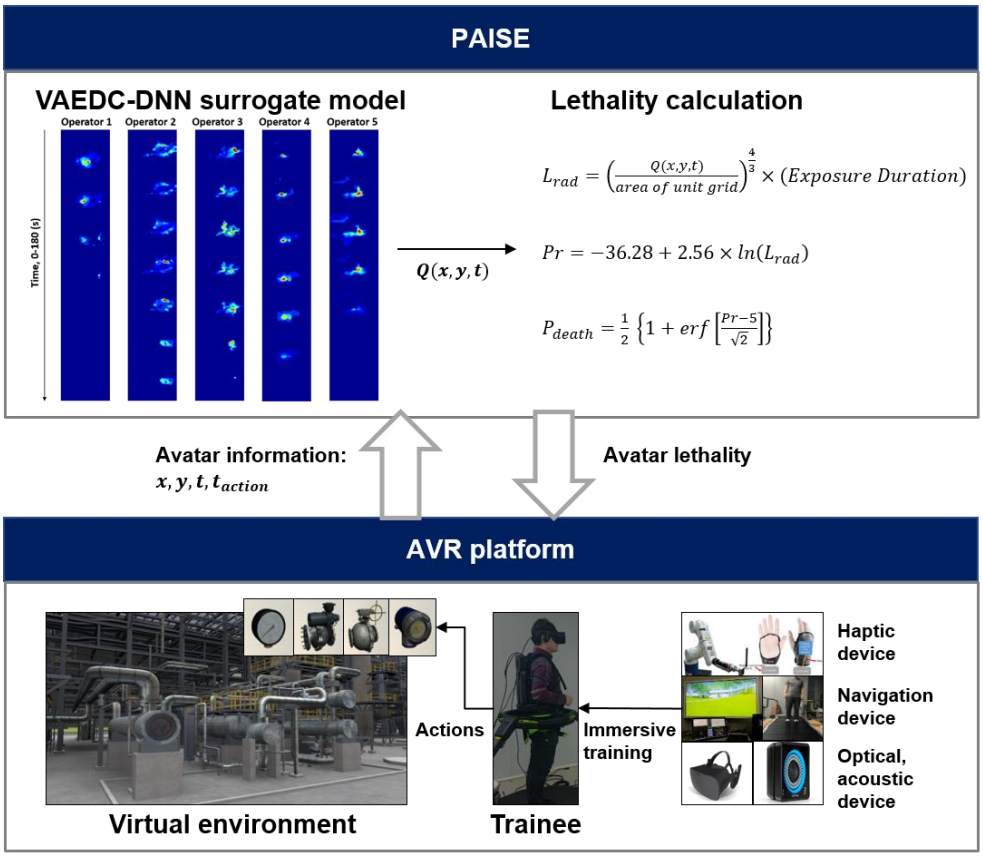

Figure 4-8. Integration of surrogate model-based accident results to AVR-based OTS

4.6. Conclusion

In this study, the CFD model was reduced and regression was performed with a surrogate model for real-time application of accident results to an AVR-based OTS. A variational autoencoder with deep convolutional layers was adopted as a means of achieving the goal. The proposed model consist of two parts, one is VAEDC: dimensionality reduction of input images to the latent space and the other is DNN: regression of four-dimensional input space of wind speed, wind direction, release duration, and time steps as mapping to the latent space. Other surrogate models were also constructed to compare the performance of the proposed model and as a result, the VAEDC-DNN model showed best performance with a minimum mean squared error. The target of this study is HOD process in the city of Seosan, South Korea, which is likely to subject to frequent accidents due to harsh operating conditions. The proposed surrogate model is expected to make the training procedure more efficient, and consequently, reduce the damage of potential catastrophic accidents in advance.

Chapter 5. Concluding remarks

In this paper, several methodologies for safer and more reliable operation of the HOD process. First, a dynamic process simulation of the reactor section in the HOD process and a subsequent QRA was implemented to identify potential risks which are undetectable by the conventional method. Potential hazards were estimated qualitatively near the reactor which have high operation pressure and temperature conditions and dynamic process simulation was conducted to identify potential hazards quantitatively during a shut-down process. Several points were found to be more dangerous than the steady-state, and a QRA was performed using those values of newly detected points. Secondly, development of interactive simulation platform which will be used as an internal engine of operator training system targeting at HOD process was conducted and simple examples were shown. Developed model was designed to take correct and prompt measures depending on the process upsets and accident scenarios via OLE. Lastly, the CFD model was reduced and regression was performed with a surrogate model for real-time application of accident results to an AVR-based OTS. A variational autoencoder with deep convolutional layers was adopted as a means of achieving the goal. The proposed model consist of two parts, the former serves as dimensionality reduction of input images to the latent space and the latter serves as regression of four-dimensional input space of wind speed, wind direction, release duration, and time steps as mapping to the latent space. The model was integrated with the AVR-based OTS, expected to produce more efficient and improved training effects.

Acknowledgement

This research was supported by a grant (19IFIP-B087592-06) from Smart Civil Infrastructure Research Program funded by Ministry of Land, Infrastructure and Transport (MOLIT) of the Korean government and Korea Agency for Infrastructure Technology Advancement (KAIA)

References

[1] R.A. Freeman, CCPS guidelines for chemical process quantitative risk analysis, Plant/Operations Progress, 9 (1990) 231-235.
[2] S.N. Jonkman, P.H.A.J.M. van Gelder, J.K. Vrijling, An overview of quantitative risk measures for loss of life and economic damage, Journal of Hazardous Materials, 99 (2003) 1-30.
[3] H. Pasman, G. Reniers, Past, present and future of Quantitative Risk Assessment (QRA) and the incentive it obtained from Land-Use Planning (LUP), Journal of loss prevention in the process industries, 28 (2014) 2-9.
[4] J.S. Arendt, Using quantitative risk assessment in the chemical process industry, Reliability Engineering & System Safety, 29 (1990) 133-149.
[5] F.I. Khan, R. Sadiq, T. Husain, Risk-based process safety assessment and control measures design for offshore process facilities, Journal of hazardous materials, 94 (2002) 1-36.
[6] N. Khakzad, F. Khan, P. Amyotte, Safety analysis in process facilities: Comparison of fault tree and Bayesian network approaches, Reliability Engineering & System Safety, 96 (2011) 925-932.
[7] P. Middha, O.R. Hansen, J. Grune, A. Kotchourko, CFD calculations of gas leak dispersion and subsequent gas explosions: validation against ignited impinging hydrogen jet experiments, Journal of hazardous materials, 179 (2010) 84-94.
[8] S. Jung, D. Ng, C. Diaz-Ovalle, R. Vazquez-Roman, M.S. Mannan, New approach to optimizing the facility siting and layout for fire and explosion scenarios, Industrial & Engineering Chemistry Research, 50 (2011) 3928-3937.
[9] I. Yet-Pole, C.-M. Shu, C.-H. Chong, Applications of 3D QRA technique to the fire/explosion simulation and hazard mitigation within a naphtha-cracking plant, Journal of Loss Prevention in the Process Industries, 22 (2009) 506-515.
[10] J. Di Domenico, C.A. Vaz Jr, M.B. de Souza Jr, Quantitative risk assessment integrated with process simulator for a new technology of methanol production plant using recycled CO2, Journal of hazardous materials, 274 (2014) 164-172.
[11] Y. Lee, S. Lee, S. Shin, G. Lee, J. Jeon, C.-J. Lee, C. Han, Risk-based process safety management through process design modification for gas treatment unit of gas oil Separation plant, Industrial & Engineering Chemistry Research, 54 (2015) 6024-6034.
[12] W.L. Luyben, Use of dynamic simulation for reactor safety analysis, Computers & Chemical Engineering, 40 (2012) 97-109.
[13] M. Shacham, N. Brauner, M.B. Cutlip, Open architecture modelling and simulation in process hazard assessment, Computers & Chemical Engineering, 24 (2000) 415-421.
[14] Z. Švandová, L. Jelemenský, J. Markoš, A. Molnár, Steady states analysis and dynamic simulation as a complement in the HAZOP study of chemical reactors, Process Safety and Environmental Protection, 83 (2005) 463-471.
[15] H.H. Lou, J. Chandrasekaran, R.A. Smith, Large-scale dynamic simulation for security assessment of an ethylene oxide manufacturing process, Computers &

chemical engineering, 30 (2006) 1102-1118.
[16] S. Eizenberg, M. Shacham, N. Brauner, Combining HAZOP with dynamic simulation—applications for safety education, Journal of Loss Prevention in the Process Industries, 19 (2006) 754-761.
[17] A. Trujillo, W.S. Kessler, R. Gaither, Common Mistakes When Conducting a HAZOP and How to Avoid Them, Chemical engineering, 122 (2015) 54-58.
[18] J.L. Fuentes-Bargues, C. González-Gaya, M.C. González-Cruz, V. Cabrelles-Ramírez, Risk assessment of a compound feed process based on HAZOP analysis and linguistic terms, Journal of Loss Prevention in the Process Industries, 44 (2016) 44-52.
[19] F. Berdouzi, C. Villemur, N. Olivier-Maget, N. Gabas, Dynamic simulation for risk analysis: Application to an exothermic reaction, Process Safety and Environmental Protection, 113 (2018) 149-163.
[20] S. Dan, C.J. Lee, J. Park, D. Shin, E.S. Yoon, Quantitative risk analysis of fire and explosion on the top-side LNG-liquefaction process of LNG-FPSO, Process Safety and Environmental Protection, 92 (2014) 430-441.
[21] M.S. Mannan, Y. Wang, H.H. West, QRA study of an activated carbon filter safeguard system, in: INSTITUTION OF CHEMICAL ENGINEERS SYMPOSIUM SERIES, Institution of Chemical Engineers; 1999, 2003, pp. 683-692.
[22] E.J. Bernechea, J.A. Vílchez, J. Arnaldos, A model for estimating the impact of the domino effect on accident frequencies in quantitative risk assessments of storage facilities, Process Safety and Environmental Protection, 91 (2013) 423-437.
[23] L. Gooijer, N. Cornil, C. Lenoble, An international comparison of four quantitative risk assessment approaches—A benchmark study based on a fictitious LPG plant, Process safety and environmental protection, 90 (2012) 101-107.
[24] OGP, Risk Assessment Data Directory, International Association of Oil & Producers, 434 (2010).
[25] R. Stryjek, J. Vera, PRSV: An improved Peng—Robinson equation of state for pure compounds and mixtures, The canadian journal of chemical engineering, 64 (1986) 323-333.
[26] Ignition probability review, model development and look-up correlations, Energy Institute, (2006).
[27] Reducing risks, protecting people: HSE's decision-making process, HSE, Health & Safety Executive, (2001).
[28] H.-R. Gye, S.-K. Seo, Q.-V. Bach, D. Ha, C.-J. Lee, Quantitative risk assessment of an urban hydrogen refueling station, International Journal of Hydrogen Energy, 44 (2019) 1288-1298.
[29] Investigation Report: Refinery explosion and fire, U.S. Chemical Safety and Hazard Investigation Board, 2005-04-I-TX (2007).
[30] A. Antonovsky, C. Pollock, L. Straker, Identification of the human factors contributing to maintenance failures in a petroleum operation, Human factors, 56 (2014) 306-321.
[31] T.A. Kletz, Making safety second nature, Process Safety Progress, 17 (1998) 196-199.

[32] L. Marcano, F.A. Haugen, R. Sannerud, T. Komulainen, Review of simulator training practices for industrial operators: How can individual simulator training be enabled?, Safety Science, 115 (2019) 414-424.
[33] S. Morgan, S. Sendelbach, W. Stewart, Improve process training with dynamic simulation, Hydrocarbon Processing;(United States), 73 (1994).
[34] A. Operator, Consider dynamic simulation tools when planning new plant startup, Hydrocarbon processing, (2003).
[35] C. Siminovich, S. Joao, Dynamic operator training simulators for sulphuric acid, phosphoric acid, and DAP production units, Procedia Engineering, 83 (2014) 215-224.
[36] P.V. Carvalho, M.C. Vidal, E.F. de Carvalho, Nuclear power plant communications in normative and actual practice: A field study of control room operators' communications, Human Factors and Ergonomics in Manufacturing & Service Industries, 17 (2007) 43-78.
[37] M. Cha, S. Han, J. Lee, B. Choi, A virtual reality based fire training simulator integrated with fire dynamics data, Fire Safety Journal, 50 (2012) 12-24.
[38] J. Cibulka, P. Mirtaheri, S. Nazir, D. Manca, T.M. Komulainen, Virtual Reality Simulators in the Process Industry: A Review of Existing Systems and the Way Towards ETS, in: Proceedings of The 9th EUROSIM Congress on Modelling and Simulation, EUROSIM 2016, The 57th SIMS Conference on Simulation and Modelling SIMS 2016, Linköping University Electronic Press, 2018, pp. 495-502.
[39] D. Manca, S. Brambilla, S. Colombo, Bridging between virtual reality and accident simulation for training of process-industry operators, Advances in Engineering Software, 55 (2013) 1-9.
[40] S. Nazir, A. Kluge, D. Manca, Can immersive virtual environments make the difference in training industrial operators, Proceedings of the Human Factors and Ergonomics Society Europe, (2014) 251-265.
[41] S.R. Hanna, M.J. Brown, F.E. Camelli, S.T. Chan, W.J. Coirier, O.R. Hansen, A.H. Huber, S. Kim, R.M. Reynolds, Detailed simulations of atmospheric flow and dispersion in downtown Manhattan: An application of five computational fluid dynamics models, Bulletin of the American Meteorological Society, 87 (2006) 1713-1726.
[42] S.R. Hanna, O.R. Hansen, S. Dharmavaram, FLACS CFD air quality model performance evaluation with Kit Fox, MUST, Prairie Grass, and EMU observations, Atmospheric Environment, 38 (2004) 4675-4687.
[43] K.J. Long, F.J. Zajaczkowski, S.E. Haupt, L.J. Peltier, Modeling a Hypothetical Chlorine Release on a College Campus, JCP, 4 (2009) 881-890.
[44] K. Palmer, M. Realff, Optimization and validation of steady-state flowsheet simulation metamodels, Chemical Engineering Research and Design, 80 (2002) 773-782.
[45] T. Chen, K. Hadinoto, W. Yan, Y. Ma, Efficient meta-modelling of complex process simulations with time–space-dependent outputs, Computers & chemical engineering, 35 (2011) 502-509.
[46] K. Wang, T. Chen, S.T. Kwa, Y. Ma, R. Lau, Meta-modelling for fast analysis of CFD-simulated vapour cloud dispersion processes, Computers & Chemical

Engineering, 69 (2014) 89-97.
[47] Y. Loy, G. Rangaiah, S. Lakshminarayanan, Surrogate modelling for enhancing consequence analysis based on computational fluid dynamics, Journal of Loss Prevention in the Process Industries, 48 (2017) 173-185.
[48] O.T. Kajero, T. Chen, Y. Yao, Y.-C. Chuang, D.S.H. Wong, Meta-modelling in chemical process system engineering, Journal of the Taiwan Institute of Chemical Engineers, 73 (2017) 135-145.
[49] J. Masci, U. Meier, D. Cireşan, J. Schmidhuber, Stacked convolutional auto-encoders for hierarchical feature extraction, in: International Conference on Artificial Neural Networks, Springer, 2011, pp. 52-59.
[50] J. Geng, J. Fan, H. Wang, X. Ma, B. Li, F. Chen, High-resolution SAR image classification via deep convolutional autoencoders, IEEE Geoscience and Remote Sensing Letters, 12 (2015) 2351-2355.
[51] D.P. Kingma, M. Welling, Auto-encoding variational bayes, arXiv preprint arXiv:1312.6114, (2013).
[52] A. Géron, Hands-on machine learning with Scikit-Learn and TensorFlow: concepts, tools, and techniques to build intelligent systems, " O'Reilly Media, Inc.", 2017.
[53] X. Glorot, Y. Bengio, Understanding the difficulty of training deep feedforward neural networks, in: Proceedings of the thirteenth international conference on artificial intelligence and statistics, 2010, pp. 249-256.
[54] S. Ioffe, C. Szegedy, Batch normalization: Accelerating deep network training by reducing internal covariate shift, arXiv preprint arXiv:1502.03167, (2015).
[55] D.P. Kingma, J. Ba, Adam: A method for stochastic optimization, arXiv preprint arXiv:1412.6980, (2014).
[56] I.M. Rezazadeh, X. Wang, M. Firoozabadi, M.R.H. Golpayegani, Using affective human–machine interface to increase the operation performance in virtual construction crane training system: A novel approach, Automation in Construction, 20 (2011) 289-298.
[57] P. Middha, O.R. Hansen, I.E. Storvik, Validation of CFD-model for hydrogen dispersion, Journal of Loss Prevention in the Process Industries, 22 (2009) 1034-1038.
[58] O.R. Hansen, M. Ichard, S.G. Davis, Validation of FLACS for vapor dispersion from LNG spills: model evaluation protocol, in: Proc. 2009 Mary Kay O'Connor Process Safety Symposium, 2009.
[59] L.R. Skarsbø, An experimental study of pool fires and validation of different CFD fire models, in, The University of Bergen, 2011.
[60] B.F. Magnussen, B.H. Hjertager, On mathematical modeling of turbulent combustion with special emphasis on soot formation and combustion, in: Symposium (international) on Combustion, Elsevier, 1977, pp. 719-729.
[61] M. Stein, Large sample properties of simulations using Latin hypercube sampling, Technometrics, 29 (1987) 143-151.
[62] D. Ha, D. Park, J. Koo, K.H. Baek, C. Han, Improvement of principal component analysis modeling for plasma etch processes through discrete wavelet transform and automatic variable selection, Computers & Chemical Engineering, 94

(2016) 362-369.
[63] H.D. Jin, Y.-H. Lee, G. Lee, C. Han, Robust recursive principal component analysis modeling for adaptive monitoring, Industrial & engineering chemistry research, 45 (2006) 696-703.
[64] M. Kano, S. Hasebe, I. Hashimoto, H. Ohno, A new multivariate statistical process monitoring method using principal component analysis, Computers & chemical engineering, 25 (2001) 1103-1113.
[65] S.J. Qin, Survey on data-driven industrial process monitoring and diagnosis, Annual reviews in control, 36 (2012) 220-234.
[66] M. Misra, H.H. Yue, S.J. Qin, C. Ling, Multivariate process monitoring and fault diagnosis by multi-scale PCA, Computers & Chemical Engineering, 26 (2002) 1281-1293.
[67] G.E. Hinton, R.R. Salakhutdinov, Reducing the dimensionality of data with neural networks, science, 313 (2006) 504-507.
[68] C. Zhou, R.C. Paffenroth, Anomaly detection with robust deep autoencoders, in: Proceedings of the 23rd ACM SIGKDD International Conference on Knowledge Discovery and Data Mining, ACM, 2017, pp. 665-674.
[69] H. Shao, H. Jiang, H. Zhao, F. Wang, A novel deep autoencoder feature learning method for rotating machinery fault diagnosis, Mechanical Systems and Signal Processing, 95 (2017) 187-204.
[70] I. Goodfellow, Y. Bengio, A. Courville, Deep learning, MIT press, 2016.

Nomenclature

H_2	hydrogen molecule
H_2S	hydrogen sulfide
ρ_f	mass density of hold-up fluid [kg/m^3]
V	hold-up volume in process equipment [m^3]
M	mass flow rate [kg/h]
k	release duration [h]
$IR_{x,y}$	total individual risk per year at the point (x, y)
$IR_{x,y,i}$	risk of fatality as a result of event i at the point (x, y)
C_D	discharge coefficient
A_o	cross-sectional area of orifice [m^2]
u_o	orifice velocity [m/s]
v_o	specific volume [m^3/kg]
$F_{w,i}$	resistance due to walls [N]
$F_{o,i}$	resistance due to sub-grid obstructions [N]
σ_{ij}	stress tensor [N/m^3]
μ_{eff}	effective viscosity [Pa·s]
μ	turbulent viscosity [Pa·s]
δ_{ij}	Kronecker delta function
C_μ	constant in the k-ε equation
ε	dissipation of turbulent kinetic energy [m^2/s^3]
k	turbulent kinetic energy [m^2/s^2]
Q	total heat flux [W/m^2]
Δx_i	length of cell in i-direction
Δt	simulation time step
z	latent space
N_z	the number of latent variables
$p_\theta(x\|z)$	probabilistic decoder as generator with parameter θ
$q_\phi(z\|x)$	probabilistic encoder with parameter ϕ
v	variable space
$\mathcal{L}(\theta, \phi; x^{(i)})$	variational lower bound
D_{KL}	Kullback-Leibler divergence
$l(\theta, \phi; x^{(i)})$	loss function
N_{train}	the number of training data set
N_v	the number of variables

Abbreviations

QRA	quantitative risk assessment
HOD	heavy oil desulfurization
ALARP	as low as reasonably practicable
IR	individual risk
SR	societal risk
OTS	operator training system
CROP	control room operator
FOP	field operator
VR	virtual reality
AVR	augmented virtual reality
CFD	computational fluid dynamics
PCA	principal component analysis
AE	autoencoder
VAE	variational autoencoder
CNN	convolutional neural network
DNN	deep neural network
CFL	Courant-Friedrich-Levy

Abstract in Korea（국문초록）

공정 안전은 사고 발생시 막대한 피해로 인하여 화학 공장을 관리하는 가장 중요한 요소 중 하나로 간주되어왔다. 이러한 목표를 달성하기 위해 위험 및 운전성 연구, 보호 계층 분석, 사건 나무 분석, 나비 넥타이 분석, 그리고 정량적 위험성 평가와 같은 다양한 연구에 의해 몇가지 방법론이 도입되었다. 위에서 언급한 방법론은 일반적으로 각각의 공정 혹은 사고 정보를 제공할 수 있는 상용 소프트웨어에 의해 수행된다. 그러나 공정과 사고는 서로 밀접하게 연관되어 있으므로 두 모듈을 통합하여 정량적이고 정확하게 계산된 위험 결과를 산출하여 공정 관리의 신뢰성을 높일 필요가 있다. 따라서 본 논문에서는 공정과 사고 시뮬레이션을 통합하여 탈황 공정을 관리하는 새로운 방법론을 제안한다.

먼저, 기존의 방법으로는 감지할 수 없는 고유한 위험을 발견하기 위하여 동적 공정 시뮬레이션 및 사고 시뮬레이션과 통합된 정량적 위험성 평가 방법론이 제안된다. 이를 위해 탈황 공정에서 공정 종료 (Shut-down) 절차의 동적 공정 시뮬레이션을 실시하여 변수의 거동을 관찰하고 이를 통하여 정상상태에서 발견할 수 없었던 운전조건들을 찾아내어 정량적 위험성 평가를 수행한다.

두번째로 탈황 공정을 안전하게 관리하기 위하여 공정과 사고 시뮬레이션 결과 데이터 전송을 통해 제어실 운전원과 현장 운전원의 협력을 목표로 하는 새로운 운전원 훈련 시스템이 도입된다. 이 대화형 시뮬레이션

모듈은 화학 공장에서 발생할 수 있는 여러가지 시나리오를 미리 상정한다. 시나리오가 시작되면 제어실 운전원과 현장 운전원의 협업을 통하여 적절한 조치를 취하도록 유도되는데 이 과정에서 공정과 사고 시뮬레이션이 연동된다. 사고 결과는 전산 유체 역학을 사용하여 정확하게 계산되며 결과를 데이터베이스에 저장하여 훈련자들의 조치에 따라서 결과를 실시간으로 불러올 수 있는 구조로 되어있다.

마지막으로 막대한 용량의 데이터베이스를 대체하기 위하여 차원 축소 및 회귀 모델이 결합된 대리 모델이 제안된다. 이러한 과정을 통하여 입력 변수는 효과적으로 잠재 공간에 투영되어 효과적인 회귀 모델이 완성되었으며 이를 통하여 전산 유체 역할을 대신할 대리 모델이 성공적으로 개발되었다.

주요어: 탈황 공정; 동적 공정 시뮬레이션; 정량적 위험성 평가; 운전원 훈련 시스템; 전산 유체 역학; 대리 모델; 확률성 암호화기

학번: 2015-21036

감사의 글

갓 입학하여 고등학생 티를 벗지 못하고 강의실을 찾아 기웃거리던 때가 엊그제 같은데 벌써 10년이라는 시간이 지나 관악에서의 생활을 마무리할 때가 다가왔습니다. 학위취득을 위하여 수학하는 동안 도움을 주신 분들께 이 지면을 빌어 감사의 말씀을 전하고자 합니다.

졸업 후 진로에 대하여 항상 고민이 많았던 저를 늘 진심으로 대해주시고 품어주신 저의 지도교수님이신 이원보 교수님께 가장먼저 감사의 말씀을 올립니다. 교수와 학생의 관계가 아득히 멀다고 생각했던 저의 편견을 깨주신 교수님의 따듯한 말씀 덕분에 장애물이 많았던 대학원 생활을 무사히 마칠 수 있었습니다. 부족한 제가 힘을 내서 학위과정을 잘 마칠 수 있었던 가장 큰 원동력이었습니다. 자주 찾아 뵙고 인사드리겠습니다.

제가 화학공정 분야에 입문하여 지금까지 이르는 데에 가장 큰 도움을 주신 한종훈 교수님께 감사의 말씀을 드립니다. 대학원 진학 후 갈팡질팡하던 시기에 교수님께서 말씀해주신 조언들을 귀담아 들으며 흔들렸던 마음을 다잡을 수 있었습니다. 교수님과 함께 다양한 프로젝트들을 진행하면서 제 자신에 대한 자신감을 키울 수 있었고 덕분에 지금의 제가 이루어졌다고 생각합니다. 무엇보다 엔지니어로서의 산업을 바라보는 시각을 교수님을 통해 확립할 수 있었습니다. 교수님을 실망시켜드리지 않고 훌륭한 엔지니어가 되도록 앞으로도 정진하겠습니다. 다시한번 감사드립니다.

제가 화학생물공학부에 입학하여 화학공정 분야에 입문할 결심을 하게 만들어주신 윤인섭 교수님께 감사의 말씀을 드립니다. 공부할 과목은 많고 시험에 채여서 미래에 대한 진지한 생각을 할 여유도 없던 학부생 시절에 교수님을 보면서 공정시스템 분야에 대한 꿈을 키우게 되었습니다. 대학원 입학 후에도 교수님이 닦아놓으신 공정시스템이라는 길을 따라가는 매 순간마다 이 길을 만드시기 위하여 숱한 고생을 하셨을 교수님께 항상 감사한 마음을 가지고 살았습니다. 엔지니어의 가치관 뿐만 아니라 사회생활에서 주의해야하는 여러가지 조언들을 저에게 말씀해주신점 아직도 가슴속에 품고 있습니다. 나무가 아닌 숲을 볼 수 있는 사람으로 성장하도록 하겠습니다. 감사합니다.

저의 학위심사를 관장해주셨던 이종민 교수님께 감사의 말씀을 드립니다. 연구분야 뿐 아니라 사적으로도 저희 연구실과 가장 가까워서 세미나를 통해 자주 뵙고 배울 수 있어서 영광이었습니다. 수업 외에 개인적으로 지도를 받은 경험은 부족하지만 그간 대학원 생활을 하면서 보고 들은 교수님의 지도 철학과, 교수님 연구 분야에서의 탁월하신 능력을 진심으로 본받고 싶습니다. 감사합니다.

다년 간 프로젝트를 함께 수행하며 개인연구 또한 열정적으로 지도해주신 임영섭 교수님께 감사의 말씀을 드립니다. 제가 교수님과 연구실에서 함께 생활한 적은 없었지만 아끼는 후배로 격없이 대해주셔서 정말 감사했습니다. 대학원 초년 시절, 철도 없고 업무수행 능력도 부족하여

교수님을 고생시켜드린 것 같아서 아직도 죄송스런 마음이 한편에 남아 있습니다. 제 대학원 시절의 전부인 프로젝트를 교수님과 함께 할 수 있어서 정말 영광이었습니다. 졸업 후에도 자주 연락드리겠습니다. 감사합니다.

제가 마지막에 논문을 쓸 수 있게 연구 여건을 제공하여 주신 이철진 교수님께 감사의 말씀을 드립니다. 교수님과 처음 함께 공부하기 시작하면서 정말 즐거웠습니다. 대학원 초년 시절에 연구실 선배로서 갖추어야 할 기본 소양들을 교수님을 보면서 배웠습니다. 때로는 연구실 선배로서 든든히 격려해주셔서 감사했습니다. 교수님 덕분에 대학원 시절 내내 자신감을 가지고 누구보다 열정적으로 생활할 수 있었습니다. 감사합니다.

지난 5년동안 학위과정을 무사히 마칠 수 있게 도와주신 연구실 가족 여러분에게도 감사의 말씀을 드립니다. 먼저 연구실 입학 당시에 가장 큰 형으로 모범이 되어주신 웅이형, 엄청난 덩치 때문에 처음에 엄청 겁먹었던 영수형, 막 입학한 제가 버릇없이 까불어도 언제나 귀엽게 받아주셔서 감사합니다. 학번 차이가 많이 남에도 불구하고 저한테 친형처럼 잘 대해주셨던 하형이형, 졸업학기에 많은 도움을 주셔서 감사합니다. 아는 것이 정말 많은 정남이형, 연구관련해서 제가 궁금한 것이 있을 때 본인 일처럼 자세하게 답변해주셔서 감사합니다. 누구보다 따뜻하셨던 대근이형, 롯데팬이여서 같이 야구보러 자주 갔었는데 이제 사는곳도 가까우니 앞

으로도 종종 야구보자고 연락드리겠습니다. 신입생 시절부터 많은 시간을 같이했던 안전팀 대선배인 정우형, 시엽이형에게도 감사의 말씀을 드립니다. 연구실 초기에 진로에 대하여 걱정하던 저에게 그 때 해주신 조언들 덕분에 연구실 생활을 잘 마무리할 수 있었습니다. 연구실 방장과 분위기 메이커 역할을 기가 막히게 잘하셨던 재흠이형, 형의 유머감각을 배우고 싶었는데 결국 졸업할 때까지 이루지는 못했네요 앞으로도 졸졸 따라다니면서 배우도록 하겠습니다. 언제나 듬직한 익환이형에게도 감사의 말씀을 드립니다. 처음에 버릇없고 철없어서 형한테 많이 혼났었는데 시간이 지나면서 점점 나아지고 있다는 형의 칭찬에 정말 기분이 좋았습니다. 형 덕분에 어디가도 1인분은 하면서 살 수 있을거 같네요. 연구실의 엄마 성호형에게도 감사의 말씀을 드립니다. 형의 성실하고 열정적인 모습을 본받아 연구가치관을 확립할 수 있었고 무사히 졸업할 수 있는 원동력이 되었습니다. 연구실의 정신적 지주 종걸이형, 형의 많은 조언들이 저의 연구 방향성을 잡아주었습니다. 최근 교수 임용도 잘 풀려서 정말 다행이고 축하드립니다. 앞으로 개고기 먹으러 자주 다녀요! 저한테 자리 정리하는 법을 알려주신 서린누나, 덕분에 지금은 처음보다는 인간처럼 치우고 살고 있습니다. 누나덕분에 수명이 5년은 늘어났을거 같아요. 감사합니다. IPS의 홍일점이면서 능력도 정말 뛰어났던 진주누나, 나중에는 방장일도 하시느라 고생 많이하셨는데 누나의 책임감 있는 모습에 많은 것을 배웠습니다. 저의 영원한 정신적 지주 용석이형! 형은 어떤 수식어로

도 형언할 수 없을 만큼 제가 존경하는거 아시죠? 연구실의 처음과 끝을 함께해주신 형에게 항상 감사하면서 살고 있습니다. 졸업하고도 자주 연락드릴게요! 그리고 존경하는 경수형, 덤벙대는 후배 연구지도 하느라 정말 고생 많으셨습니다. 늘 따뜻한 말씀 해주셔서 감사합니다. 형수님이랑도 백년해로 하시기 바랍니다. 연구실의 야근왕 건희형, 늘 활기차게 사시고 주변사람들을 격려해주시는 형의 모습에서 많은 것을 배웠습니다. 저도 형의 그런 모습을 보면서 연구실 생활을 즐겁게 할 수 있었습니다. 연구실의 고품격 술거지 창수형, 준모형, 원제, 건학에게도 감사하다는 말씀을 드립니다. 여러분들 덕분에 퇴근시간을 항상 기다렸었고 지루한 대학원 생활에 큰 활력소가 되었습니다. 연구실의 똑똑이 창환이, 과묵해서 얼마 안하는 말 몇마디에 뼈가 있었던 너의 대화법은 지금도 배울라고 하는데 잘 안되네. 졸업하고 나서도 종종보면서 가르쳐 줬으면 좋겠다. 졸업할 때 정말 도움을 받았던 영근이형, 연구분야가 비슷해서 많이 귀찮게 해드렸는데 앞으로도 그럴 예정이니 자주 연락 드리겠습니다. 정말 감사합니다. 연구실의 재간둥이 경우, 맡은 업무는 최소한의 노력으로 최대한의 성과를 뽑아내는 너의 업무 처리 방식을 보면서 정말 많이 배웠어. 이제 졸업했으니까 여행도 종종 다니고 그러자. 그리고 동기이면서도 정말 존경하는 담대, 민준, 성언이에게도 고맙다는 말을 전합니다. 너네들 보면서 많은 동기부여가 됐던 것 같아. 앞으로도 진로 관련해서 자주 연락하고 조언을 구했으면 좋겠다. 정말 고마웠어! 연구실 후배이면서

인생 선배였던 호동이형! 형에게는 정말 빚진게 많네요. 형이 햅틱팀 후배로 들어와서 너무 행복했습니다. 형이 없었으면 지금의 저는 없었을 거에요. 졸업 후에도 자주 봤으면 좋겠습니다. 아끼는 또 한명의 햅틱팀 후배 동주, 이과제 저과제 옮겨다니느라 햅틱도 오래는 못했지만 네가 도와준 덕분에 과제를 잘 마무리할 수 있었어. 정말 고마워. 마지막에 정말 많은 도움을 준 종민이와 재훈이에게도 고맙다는 말을 전합니다. 오히려 제가 후배라고 느낄만큼 여러 방면에서 제가 배울점이 많았습니다. 앞으로 분당 자주 놀러와! 믿음직한 후배 동우형, 어른스러운 형한테 가끔 칭얼댔던거 같은데 그때마다 잘 받아주셔서 감사합니다. 이외에 아끼는 후배들. 솔지, 철원, 정용, 현기에게도 감사의 말씀을 드립니다.

힘들거나 즐거울 때 언제나 함께했었고 앞으로도 함께할 나의 소중한 대학동기 준범, 지헌, 종우, 준식, 상훈, 의석 모두 고맙고 사랑합니다.

그리고 나의 이십대 중후반의 대부분을 함께한 대중이에게도 고맙다는 말을 전합니다. 대중아, 앞으로는 지금보다 더 자주봤으면 좋겠다.

마지막으로 지금의 나를 살아올 수 있도록 함께 믿고 응원해주신 가족들에게도 진심 어린 감사의 말씀을 올립니다. 사랑합니다.

2020년 1월 서울대학교 302동 617호 연구실 내자리에서

고 창 준